Structure of apolipoprotein B-100 in low density lipoproteins

Jere P. Segrest,[1,*,†,††] **Martin K. Jones,**[*,††] **Hans De Loof,**[††] **and Nassrin Dashti**[§,**]

Departments of Medicine,* Biochemistry and Molecular Genetics,† Nutrition Sciences,§ and Pediatrics,** and the Atherosclerosis Research Unit,†† 630 Boshell Bldg., #3, UAB Medical Center, Birmingham, AL 35294-0012

Abstract   There is general consensus that amphipathic α-helices and β sheets represent the major lipid-associating motifs of apolipoprotein (apo)B-100. In this review, we examine the existing experimental and computational evidence for the pentapartite domain structure of apoB. In the pentapartite nomenclature presented in this review (NH_2-βα_1-β$_1$-α$_2$-β$_2$-α$_3$-COOH), the original α$_1$ globular domain (Segrest, J. P. et al. 1994. *Arterioscler. Thromb.* 14: 1674–1685) is expanded to include residues 1–1,000 and renamed the βα_1 domain. This change reflects the likelihood that the βα_1 domain, like lamprey lipovitellin, is a globular composite of α-helical and β-sheet secondary structures that participates in lipid accumulation in the co-translationally assembled prenascent triglyceride-rich lipoprotein particles. Evidence is presented that the hydrophobic faces of the amphipathic β sheets of the β$_1$ and β$_2$ domains of apoB-100 are in direct contact with the neutral lipid core of apoB-containing lipoproteins and play a role in core lipid organization. Evidence is also presented that these β sheets largely determine LDL particle diameter. Analysis of published data shows that with a reduction in particle size, there is an increase in the number of amphipathic helices of the α$_2$ and α$_3$ domains associated with the surface lipids of the LDL particle; these increases modulate the surface pressure decreases caused by a reduction in radius of curvature. The properties of the LDL receptor-binding region within the overall domain structure of apoB-100 are also discussed. Finally, recent three-dimensional models of LDL obtained by cryoelectron microscopy and X-ray crystallography are discussed. These models show three common features: a semidiscoidal shape, a surface knob with the dimensions of the βC globular domain of lipovitellin, and planar multilayers in the lipid core that are approximately 35 Å apart; the multilayers are thought to represent cholesteryl ester in the smectic phase. These models present a conundrum: are LDL particles circulating at 37°C spheroidal in shape, as generally assumed, or are they semidiscoidal in shape, as suggested by the models? The limited evidence available supports a spheroidal shape.— Segrest, J. P., M. K. Jones, H. De Loof, and N. Dashti. **Structure of apolipoprotein B-100 in low density lipoproteins.** *J. Lipid Res.* **2001.** 42: 1346–1367.

Supplementary key words   amphipathic β sheets • amphipathic α-helices • cryoelectron microscopy • X-ray crystallography • boundary lipid • smectic phase • lipid phase transition • LDL receptor-binding domain

INTRODUCTION

Lipoproteins are submicroscopic particles composed of lipid and protein held together by noncovalent forces. Their general structure is that of a putative spheroidal microemulsion formed from an outer layer of phospholipids, unesterified cholesterol, and proteins, with a core of neutral lipids, predominately cholesteryl ester and triacylglycerols (TAG). Although the microemulsion is the basic structural motif of lipoproteins, several different lipoprotein classes exist that differ in relative amount of lipids, in the protein/lipid ratio, and in the protein species present, resulting in differences in size, density, and electrophoretic mobility. Lipoproteins are generally classified by density, size, and/or protein composition.

Apolipoproteins

Apolipoproteins are amphipathic in nature, in that they have both hydrophobic and hydrophilic regions, and can therefore interact both with the lipids of the lipoprotein and with the aqueous environment (1). Because of the nature of these amphipathic regions, apolipoproteins act as detergents, and have a major role in determining and stabilizing the size and structure of the lipoprotein particle.

Plasma apolipoproteins can be grouped into two classes, the nonexchangeable apolipoproteins [apolipoprotein (apo)B-100 and apoB-48], and the exchangeable apolipoproteins (apoA-I, apoA-II, apoA-IV, apoC-I, apoC-II, apoC-III, and apoE) (2). ApoB-100 is highly insoluble in aqueous solution and is one of the largest monomeric proteins known. On the other hand, the exchangeable apolipoproteins are soluble in aqueous solutions, and the secondary structural motif responsible for their lipid association, the amphipathic α-helix, has been extensively studied (1–3).

LDL

The only protein component of LDL is a single molecule of apoB-100 per particle (4–6). LDL, about 200 Å in diameter, is much smaller in size than the originally secreted VLDL that ranges from 600 to 800 Å. Analytical and structural studies of LDL (7–21) suggest a range of particle sizes (180–250 Å). Subfractions of LDL, characterized by variations in density, size, and chemical composition, are

---

assuming important clinical significance; a predominance of small dense LDL particles is associated with an increased risk of coronary heart disease (19, 22, 23).

LIPID-ASSOCIATING DOMAINS OF APOB-100

Amphipathic α-helical and β-strand motifs

The B apolipoproteins are highly insoluble in aqueous solutions and, thus, remain with the lipoprotein particle throughout its metabolism (24). Because of the size and insoluble nature of apoB, it has been difficult to confirm the structural motifs responsible for the lipid-associating properties of this nonexchangeable apolipoprotein (25, 26).

Circular dichroic (CD) spectroscopy of LDL suggested that apoB-100 has an α-helical content of 25% or greater (27–30). Amphipathic α-helices, the ubiquitous lipid-associating motifs in the exchangeable apolipoproteins, were detected in the sequence of apoB-100 by helical wheel analysis (5, 31). Using computer analysis, De Loof et al. (32) noted two clusters of potential 22-mer amphipathic helical repeats between residues 2,079–2,428 and 4,150–4,484. Further, they showed, using comparison matrix analysis, that the regions between residues 2,035–2,506 and 4,002–4,527 contained sequence similarity to the exchangeable apolipoproteins.

Yang et al. (33, 34) used nondissociability of peptides from trypsin-treated intact LDL to develop a map of the lipid-associating regions of apoB-100 (**Fig. 1**). They determined the regions of apoB on the LDL particle that were trypsin releasable, those that were not, and those there were mixed. Based on this criteria, five broad domains of apoB were identified. Their map defined two major apoB-100 lipid-associating domains between residues 1,701–3,070 and 4,101–4,536.

Analyzing the data of Yang et al. (33, 34) in another way, two continuous stretches of apoB-100, residues 2,100–2,700 and 4,100–4,500, contain less than 10 trypsin-releasable residues per 100 amino acid residues (35). These two regions correspond closely to the amphipathic helical repeats identified by De Loof et al. (32) between residues 2,079–2,428 and 4,150–4,484.

As first suggested by Gotto, Levy, and Fredrickson (28), apoB-100 differs from the exchangeable apolipoproteins in that it contains β-sheet structure, estimated using CD spectra of isolated LDL to be 15–25% (28, 30, 36, 37). Infrared spectroscopy, considered a better method for determining the content of β structure than CD spectroscopy, suggested as much as 41–50% β sheet in apoB-100 [(37) and V. K. Mishra et al., unpublished data].

The results of infrared spectroscopy also suggested that the β sheets of apoB-100 are oriented parallel to the phospholipid monolayer of LDL (37). Relevant to this possibility, several different research groups have postulated that amphipathic β strands contribute to the high affinity of apoB-100 for the lipid surface of VLDL and LDL (5, 35, 37–42). Significantly, Fourier analysis of amphipathic structures in apoB-100 by Nolte (42) indicated that two large regions of apoB-100 are enriched in amphipathic β strands. Supporting the concept that amphipathic β strands contribute to the lipid affinity of apoB-100, a model amphipathic β-strand peptide was synthesized and shown to have properties similar to apoB-100 (43). The computer analysis of amphipathic helical repeats by De Loof et al. (32) combined with the Fourier analysis of amphipathic β strands by Nolte (42) suggested that apoB-100 might contain four consecutive domains alternately enriched in amphipathic α-helices and amphipathic β strands.
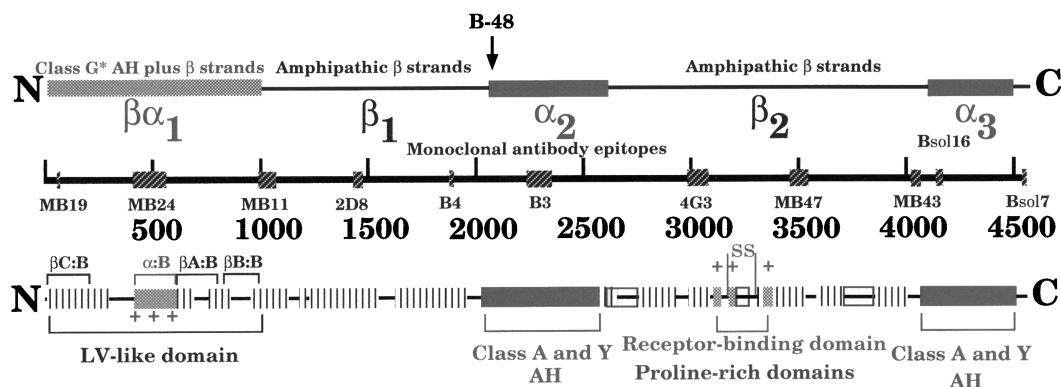
Pentapartite model

A computer program called LOCATE was developed by Segrest et al. (35) to examine the lipid-associating domains of apoB-100 in more detail. Analysis with this program confirmed the presence of two regions of amphipathic β strands alternating with two regions of amphipathic α-helices (32, 42), and suggested the presence of a third N-terminal amphipathic α-helical domain, giving apoB-100 a pentapartite structure: NH_3-α_1-β_1-α_2-β_2-α_3-COOH (**Fig. 2**). As the amphipathic α-helices of the α_1 domain were class G* (1–3), these authors proposed that the α_1 domain of apoB represented a globular region. Because the amphipathic α-helices of the α_2 and α_3 domains were mostly class A and Y (the types found in the exchangeable apolipoproteins), they proposed that these two regions of apoB-100 represented flexible domains with reversible lipid affinity. These authors further suggested that the two amphipathic β-strand domains in apoB-100 (β_1 and β_2) represented the irreversibly lipid-associated regions of this irreversibly associated apolipoprotein.

In a second publication, Segrest et al. (44) compared the complete sequence of human apoB-100 with partial
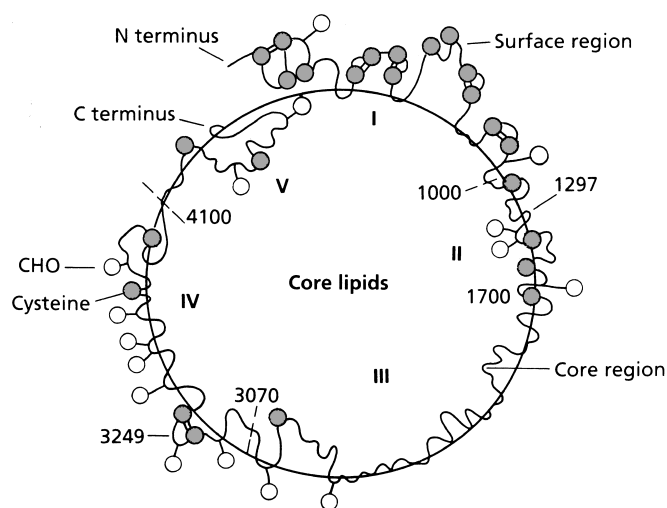
Fig. 1. Schematic diagram of the structure of apoB-100 on the surface of LDL. Trypsin-releasable and trypsin-nonreleasable regions are shown on the inside and outside of the LDL surface, respectively. The five proposed domains are demarcated by dashed lines. The two thrombin-cleavable sites are marked at residues 1,297 and 3,249. Open circles represent N-glycosylated carbohydrates, and shaded circles represent cysteine residues. Reproduced from Yang et al. (34) with permission.

Fig. 2. Schematic diagram of the pentapartite structural model, NH_3-$\beta\alpha_1$-β_1-α_2-β_2-α_3-COOH, for apoB-100. Upper: the five domains defined previously (35, 44) have been modified as follows: first, the N-terminal α_1 (globular) domain, based upon homology to lipovitellin (59), has been expanded to encompass residues 1–1,000 and, because of the presence of both amphipathic α-helical and β strands in the sequence, renamed the $\beta\alpha_1$ domain. Thus, the β_1 domain has been shortened to encompass residues 1,001–2,000. Middle: this portion of the figure shows the positions within the apoB-100 sequence of the monoclonal antibodies used by Schumaker and colleagues (60, 102) to map the location of apoB-100 onto the LDL particle surface. Bottom: this portion of the figure denotes structural details proposed for the individual pentapartite domains.

sequences from eight additional species of vertebrates. They showed that class A lipid-associating amphipathic α-helices cluster in two domains in all species for which those regions have been sequenced, but with little conservation of individual helices: α_2 between residues 2,075 ± 25 and 2,575 ± 25, and α_3 between residues 4,100 ± 100 and 4,550 ± 50. These authors further showed that amphipathic β strands cluster in two domains in all species for which these regions have been sequenced, with apparent conservation of several individual amphipathic β strands: β_1 (approximately residues 827–2,000) and β_2 (approximately residue 2,571 to residue 4,000 ± 50). Finally, they found that hydrophobic segments were present in apoB-100 sequences of all nine species, but the frequency of occurrence was no greater than generally found in β sheet-containing proteins. Analysis of the overall conservation of the α_1 domain was difficult because of limited amino acid sequence data on this domain of apoB from species other than human. It was concluded that the four alternating lipid-associating domains, -β_1-α_2-β_2-α_3-COOH, are common supramolecular features of apoB-100 in all vertebrate species (44).

Effects of apoB truncation on lipid affinity

Several laboratories have reported a number of naturally occurring apoB gene mutations that produce truncated forms of apoB that range in length from 9% (apoB-9) to 89% (apoB-89) of full-length apoB-100 (45, 46). Because many domains throughout the entire length of apoB appear to be involved in lipid binding, truncated apoB is expected to form denser lipid-poor particles. For example, Parhofer et al. (47) demonstrated that apoB-89, apoB-75, and apoB-54.8 were secreted into the VLDL fraction, whereas apoB-31 was secreted into HDL. In general, the shorter the mutant apoB protein, the denser and more lipid poor the particle (48). In fact, studies on the expression of truncated forms of apoB in cultured cells

have indicated that the size of the secreted particles and the amount of lipid per particle are proportional to the length of the truncated apoB (49–52).

Studies in mouse mammary carcinoma-derived cells by Carraway et al. (52) demonstrated that apoB-29, apoB-32.5, and apoB-37 had peak densities of 1.25, 1.22, and 1.16 g/ml, had lipid weight percentages of 30%, 37%, and 49%, and had calculated anhydrous particle diameters of 81, 88, and 101 Å, respectively. The core TAG of the apoB-29, apoB-32.5, apoB-37, and apoB-41 particles accounted for 11%, 28%, 58%, and 68%, respectively, of the total lipid mass. These investigators (52) concluded that the sequences in the C-terminus of apoB-29 bind phospholipids and diacylglycerols, sequences between apoB-29 and apoB-32.5 augment TAG binding, and sequences between apoB-32.5 and apoB-41 account for the marked incorporation of TAG at the rate of ~1 TAG per two amino acids.

Morphology of detergent-solubilized apoB-100

A recent publication by Gantz, Walsh, and Small (53) reported the shape of sodium deoxycholate-solubilized apoB-100 using cryoelectron microscopy. The majority of molecules prepared in negative stain and vitreous ice were curved and had alternating thin and thick regions. In negative stain, the apoB molecules lay on the grid perpendicular to the electron beam and had a mean length of 650 Å. In vitreous ice, the molecules measured up to 650 Å in length and showed one or two beaded regions. Similar regions were also observed in negative stain. Some vitrified molecules contained ribbon-like portions. These images suggested a long flexible beaded-thread morphology for apoB-100 (53).

Conformation of the β_1 and β_2 domains of apoB-100 on LDL particles

Although the amphipathic β strand is generally accepted as a major lipid-associating motif in apoB, little direct

evidence for its mode of association with phospholipid monolayers exists. Small and Atkinson [(54) and personal communication] analyzed the amphipathic β strands in the N-terminal half of apoB. For this analysis, they combined the Fourier power spectrum approach of Nolte and Atkinson (55) and the algorithm of White, Stultz, and Smith (56). Their analysis located 57 amphipathic β strands of 11 residues or more in B41; 41 were between residues 968 and 1,882 (B21–B41) and 47 were between B18 and B41. Most of the strands were 11-mers but several were longer, up to 15 residues in length. The 41 amphipathic β strands in B21–B41 contained over 58% of the residues. These investigators proposed (54) that this region of apoB forms a nearly continuous amphipathic β sheet. When they modeled the 41 amphipathic β strands in

B21–B41 as a continuous sheet, they calculated the total ΔG of lipid-association for the sheet to be on the order of 500 kcals/mol, an extremely high lipid affinity (54). This proposal is similar to the one by Segrest et al. (35) that the two amphipathic β-strand domains ($β_1$ and $β_2$) with, for all practical purposes, infinite lipid affinity (44), represented the irreversibly lipid-associated regions of apoB-100.

Amphipathic β strands are found in a few classes of proteins in addition to apoB. One example is the egg yolk lipoprotein, lipovitellin. **Figure 3** illustrates the molecular features of a five-stranded antiparallel amphipathic β-sheet segment, residues 1,374–1,440, from the lipid-associated nine-stranded amphipathic βD-sheet domain of lamprey lipovitellin (see **Fig. 4**). The structure of this β sheet was determined by X-ray crystallography (57, 58); the sheet
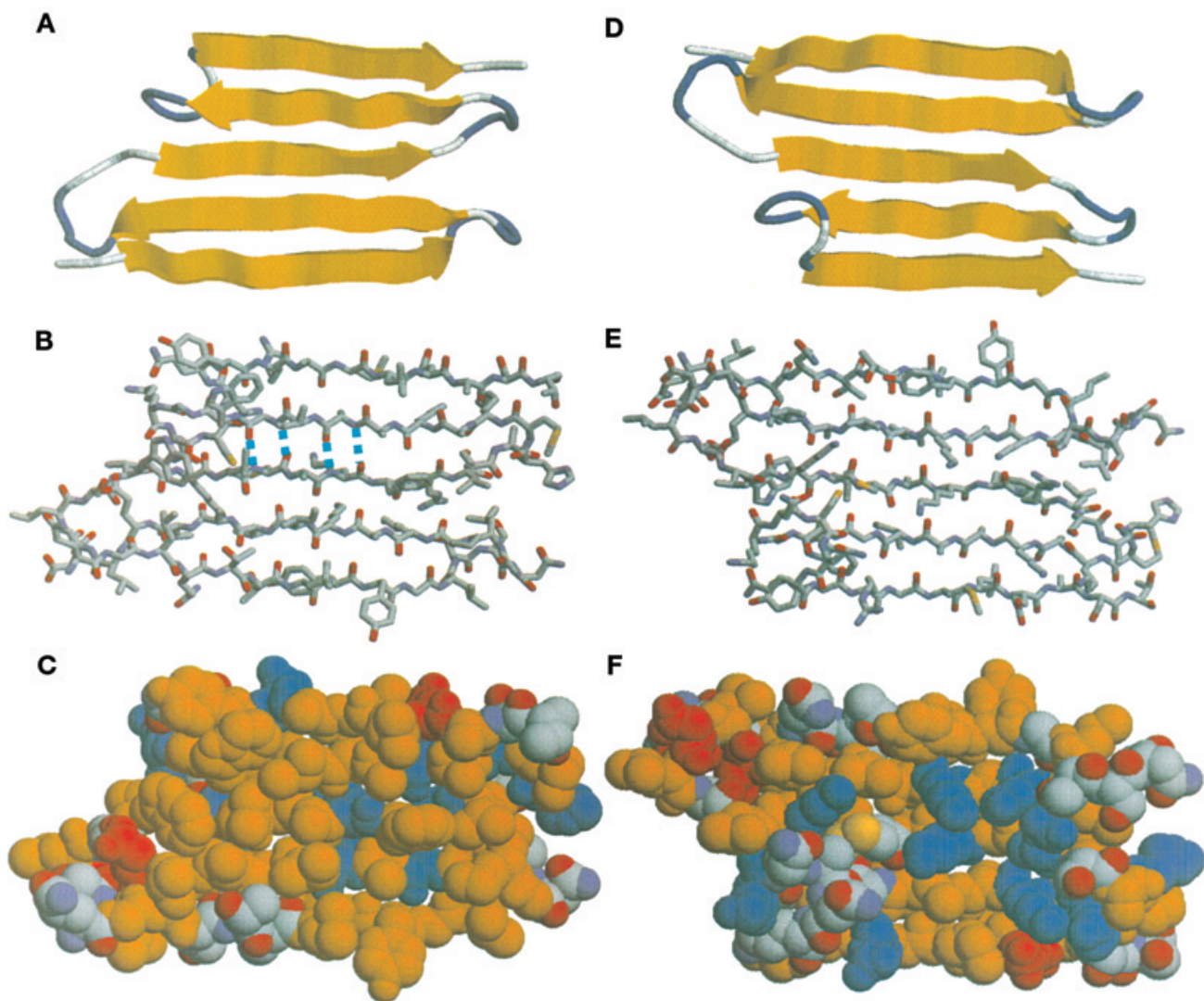
Fig. 3. Molecular models of the five-stranded antiparallel β-sheet segment (residues 1,374–1,440) from the lipid-associated nine-stranded amphipathic βD-sheet domain of lamprey lipovitellin (57, 58). A, B, and C: the β sheet is oriented with the hydrophobic face up and the N-terminal region at the bottom. D, E, and F: the β sheet is oriented with the hydrophilic face up and the N-terminal region at the bottom. A and D: the two orientations of the β sheet are displayed as cartoon models. Individual β strands are represented by arrows (gold) with the arrowhead denoting the C-terminal direction. β turns are in blue. B and E: the two orientations of the β sheet are displayed as stick-figure all-atom molecular models. In B, one set of interstrand hydrogen bonds is represented by dashed blue lines. C and F: the two orientations of the β sheet are displayed as all-atom space-filling models. Hydrophobic residues (L, I, V, M, C, A, F, W, Y) are gold, positively charged residues (K, R, H) are blue, and negatively charged residues (E, D) are red. All model views were created by the program RASMOL (145).
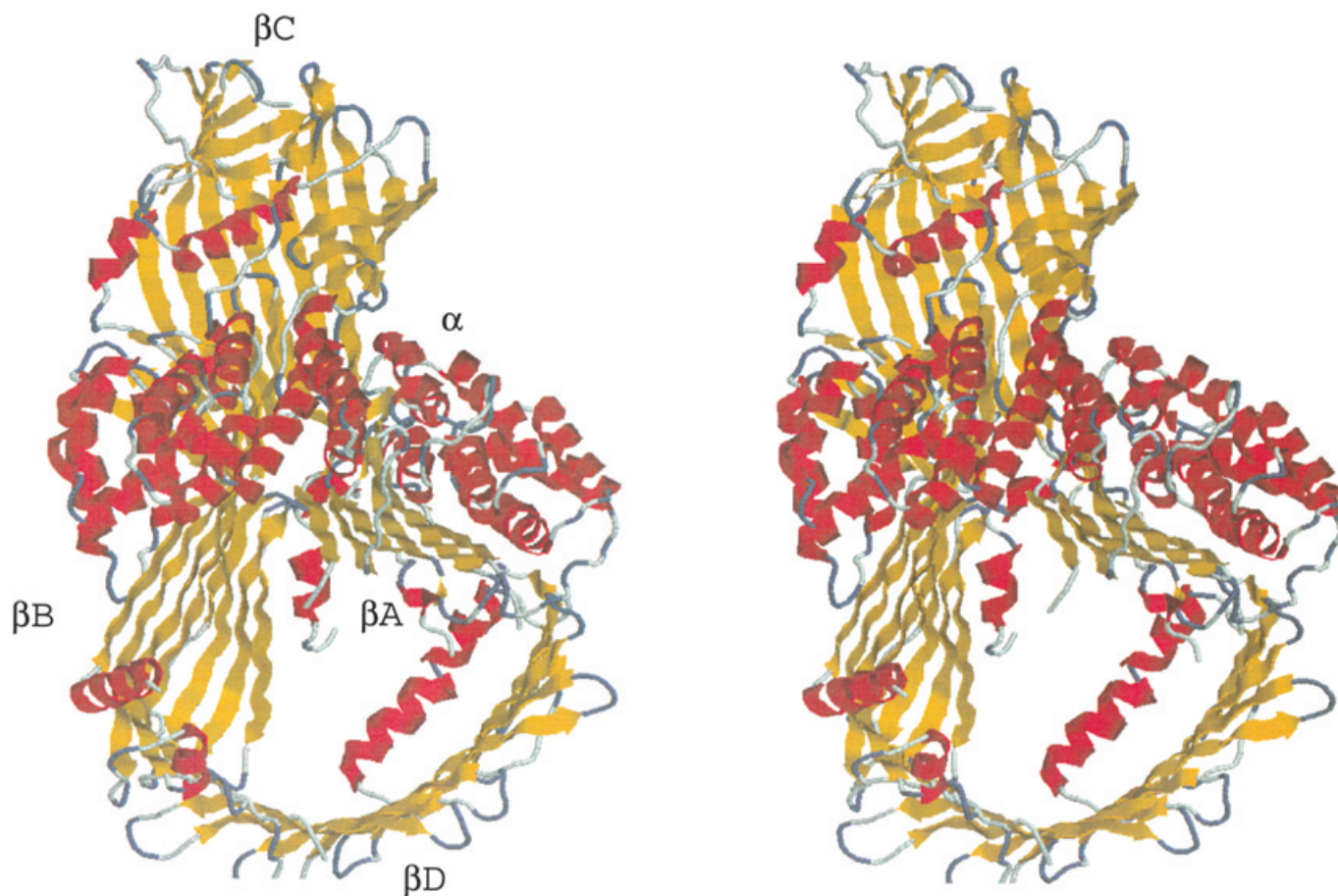
Fig. 4. Cross-eyed stereo cartoon model of lamprey lipovitellin. The coordinates of the X-ray crystal structure for lamprey lipovitellin (57, 58) were obtained from the Protein Databank. Individual β strands are represented by arrows (gold) with arrowheads denoting the C-terminal direction, α-helices are represented by red coils, and β turns are shown in blue. The four β-sheet domains of lamprey lipovitellin are labeled βC, βB, βA, and βD, and the α-helical domain is labeled α. The figure was created using the program RASMOL (145).

shown in Fig. 3 has an average of 8.5 residues per strand (to give an average sheet width of approximately 30 Å) and 6 residues per turn. In Fig. 3, the β sheet is oriented to view the hydrophobic and hydrophilic faces in the left- and right-hand columns, respectively, and is displayed as cartoon, stick, and space-filling models in the upper, middle, and lower rows, respectively. The space-filling models highlight hydrophobic residues in gold, positively charged residues in blue, and negatively charged residues in red. In the left-hand stick model, one set of interstrand hydrogen bonds is represented by dashed blue lines.

Local alignment of sequence blocks performed by the computer program MACAW (Multiple Alignment Construction and Analysis Workbench), searching by segment-pair overlap, suggested that the sequence of the β-sheet structure of lipovitellin shown in Fig. 3 possesses a weak similarity to a sequence at the N-terminal end of the β_1 domain of apoB near residue 1,150 (59). This β sheet thus represents a good working model for the proposed amphipathic β sheets of the β_1 and β_2 domains of apoB-100. A continuous amphipathic β-sheet model for the β_1 and β_2 domains of apoB-100 can explain the findings of Gantz, Walsh, and Small (53) that detergent-solubilized apoB-100

is a long thin flexible thread of about 650 Å in length that contains several ribbon-like portions.

MECHANISM OF ASSEMBLY OF APOB-CONTAINING LIPOPROTEIN PARTICLES

Background

The assembly of apoB-containing lipoprotein particles occurs co-translationally (60); that is, the C-terminal portion is synthesized on the ribosome of the endoplasmic reticulum (ER) as the N-terminal portion is assembling a small lipoprotein particle. Disulfide-dependent folding of the N-terminal domain of apoB is required for assembly (61–63). One often-quoted mechanism for the physical assembly of lipid particles containing apoB is the budding oil droplet (60). In this model, the N-terminal portion of apoB is embedded in the inner monolayer of the ER membrane where it nucleates an oil droplet from the supersaturated rough RE membranes. Upon completion of apoB synthesis, this oil droplet is detached from the bilayer to form the nascent lipoprotein. One weakness of this model is that an extensive search by electron microscopy

for inner rough ER membrane blebs in liver microsomal preparations has failed (60). Further, thermodynamic considerations make it unlikely that lipoproteins assemble through the wholesale remodeling or dismantling of membrane bilayers as suggested by the budding oil droplet model. It seems more likely that apolipoproteins accrete the lipid for their corresponding lipoprotein particles gradually (64).

The autosomal recessive disorder, abetalipoproteinemia, results in a virtual absence of apoB-containing lipoproteins, and microsomal triglyceride-transfer protein (MTP) is also not detectable (65). Although disputed by some (66), this observation has led to the suggestion that MTP is necessary for the formation of apoB-containing lipoproteins (67–69). Recent studies in cell lines that do not express apoB and MTP (i.e., HeLa and COS-1 cells) have clearly demonstrated that co-transfection of these cells with these two proteins resulted in secretion of apoB-containing lipoproteins (67, 70). Further, an inhibitor of the MTP has been shown to inhibit apoB secretion from HepG2 cells (68). Evidence to date supports the notion that initial lipidation of the nascent apoB polypeptide may occur through direct association with MTP, and that this step may be required for proper folding of the polypeptide in order to escape ubiquitination and subsequent degradation (71).

Lipid pocket model

In their comparison of apoB-100 from nine species, Segrest et al. (44) reported that a number of the amphipathic α-helices in the α_1 domain, unlike the α_2 and α_3 domains, appeared to be conserved. In a follow-up article, Segrest, Jones, and Dashti (59) reported that the first 1,000 residues of human apoB-100 (the α_1 domain plus the first 200 residues of the β_1 domain, the $\beta\alpha_1$ domain) have sequence and amphipathic motif homologies to lamprey lipovitellin. The X-ray crystal structure of lamprey lipovitellin, an egg yolk lipoprotein shown in Fig. 4 (57, 58, 72, 73), is known to contain a "lipid pocket" lined by three antiparallel amphipathic β sheets designated βB, βA, and βD. The top two amphipathic β sheets, βB and βA, are joined together by an antiparallel double-layered bundle consisting of 17 α-helices designated the α domain. The fourth β-sheet domain of lamprey lipovitellin, βC, forms a globular β barrel structure at the apex of the triangular lipid pocket.

Lipovitellin was compared to apoB-100 by Segrest, Jones, and Dashti (59) because a database search for protein sequences that contained amphipathic β strands similar to those found in apoB-100 turned up four vitellogenins, the precursor form of lipovitellin, from chicken, frog, lamprey, and *C. elegans*. Segrest, Jones, and Dashti (59) also showed that most of the α_1 domain of human apoB-100 has sequence and amphipathic motif homologies to human MTP, an observation also made by others (74–76).

Based upon their results, Segrest, Jones, and Dashti (59) suggested that a lipovitellin-like "proteolipid" intermediate containing a lipid pocket is formed by the N-terminal portion of apoB. They suggested that this intermediate produces a lipid nidus required for assembly of apoB-containing lipoprotein particles. Pocket expansion

through the addition of amphipathic β strands from the β_1 domain of apoB then results in the formation of HDL, and then in VLDL-like spheroidal particles (**Fig. 5**).

The apparent absolute requirement of MTP for assembly of apoB-containing lipoproteins could simply mean that MTP plays a purely nonstructural role as a shuttle to fill the lipid pocket of the proposed lipovitellin-like apoB intermediate. However, because MTP binds specifically to the unlipidated $\beta\alpha_1$ domain of apoB (75, 77, 78), MTP also may play a more central structural role in assembly of apoB-containing lipoproteins. Segrest, Jones, and Dashti (59) hypothesized that in the absence of the MTP, the lipovitellin-like apoB lipid pocket intermediate is incomplete, and no apoB-containing lipoprotein can be assembled (Fig. 5).

Particularly relevant in the development of a model is a study by Hussain et al. (77). They showed that positively charged amino acid residues, presumably on amphipathic α-helices located between residues 430–570 of apoB, are critical for MTP binding to apoB. Further, they found that 40% and 70% of this binding activity is abolished by truncation of the apoB:570 construct to residues 509 and 502, respectively. LOCATE identifies three positively charged amphipathic α-helices between residues 477–491, 492–508, and 527–541 in the N-terminus of the domain of apoB that are homologous to the C-terminal half of the α-helical domain lipovitellin; the locations of these three amphipathic helices, particularly the latter two, correlate extremely well with the Hussain et al. (77) data.

In another recent article, Mann et al. (75) used molecular modeling to suggest a homology of the N-terminal region of lamprey lipovitellin to the N-terminal portions of both apoB and MTP. Based upon the results of site-directed mutagenesis, these authors proposed that initial apoB binding to MTP occurs via their respective homologue domains (75). These results suggest that the β barrel structure proposed by Mann et al. (75) for the N-terminal region of apoB may be the TAG-binding domain of apoB that accepts "shuttled" monomeric TAG from the β barrel region of the N-terminal domain of MTP.

As noted earlier in this review, expression of progressively smaller C-terminal truncated forms of apoB-100 in cell culture demonstrated that near the N-terminal end of the β_1 domain, the percentage of the truncated apoB-100 associated with lipid approaches zero (48, 49, 66, 79, 80). There appears to be a threshold in apoB size (somewhere between apoB-23 and apoB-28) under which the polypeptide cannot form a lipoprotein particle. Further, McLeod et al. (80) showed that B-29 forms a HDL-like particle when expressed in McA-RH7777, but VLDL particle formation requires inclusion of multiple amphipathic β strands from the β_1 domain beyond apoB-29. Other studies have shown that the diameters of secreted lipoprotein particles are linearly proportional to the length of C-terminal truncated apoB-100 fragments until a minimal apoB fragment length is reached (49, 60); the linearity falls off near the end of the β_1 domain, between residues 1,100 and 1,300. In another study, B-17 was recovered from the media free of lipid, but when combined with
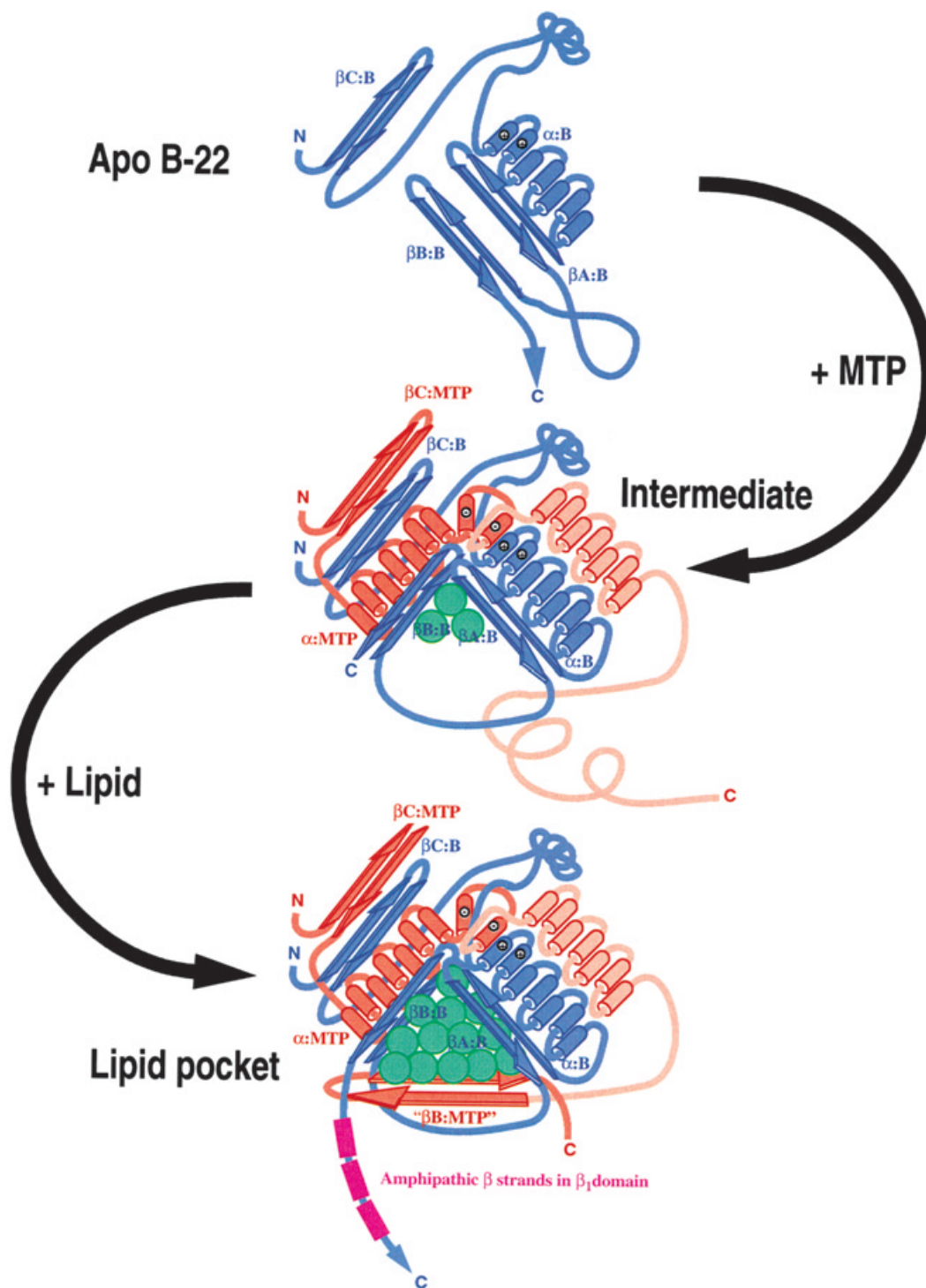
Fig. 5. Lipid pocket model for assembly of apoB-containing lipoprotein particles. Upper panel: diagrammatic model of apoB-22 (residues 1–1,000; blue) in the absence of MTP. The protein structural schematics, cylinders for α-helices, and antiparallel arrows for antiparallel β sheets indicate the relative positions of the β sheets βC:B, βA:B, and βB:B, and the α-helical cluster α:B. For simplicity, only two of the β strands in each β sheet are shown. Note the truncation of α:B to approximately half the length of α:lipovitellin. Middle panel: in the presence of MTP (red), an intermediate is formed that allows for the accretion of lipid (green circles). The α:MTP portion of hMTP (negatively charged) likely represents the domain of hMTP that binds to the positively charged N-terminal portion of the α:B domain of h-apoB (29–31). Bottom panel: upon the completion of the α:lipovitellin structure with "βD:MTP," homologous to the βD amphipathic β sheet of lipovitellin, there is complete assembly of the lipid nidus in the lipid pocket to form a proteolipid particle. ApoB is then competent to grow co-translationally thorough the addition of amphipathic β strands from the ββ₁ domain to allow the accretion of more lipid to create a true lipoprotein particle.

phospholipid, it formed discoidal complexes, suggesting the presence of amphipathic motifs within the B-17 sequence (66). Taken together, truncation studies suggest a rather abrupt change in the nature of the interactions between apoB and bulk lipid at the $\beta\alpha_1$-β_1 boundary. They support the suggestions (35, 44) that *a*) a major portion of the $\beta\alpha_1$ domain is globular and not an integral part of the bulk lipid of the apoB-containing lipoprotein particles, and *b*) the β_1 domain is extended and is integrated into the bulk lipid of these same particles.

RECEPTOR-BINDING DOMAINS OF APOB-100

Published results

As with so many other aspects of apoB-100, characterizing its interaction with the LDL receptor at a molecular level turned out to be a difficult task. When the sequence became available, it was not clear whether predictions and early experiments supported one (38), two (4), or more (81) domains interacting independently or in concert with the LDL receptor. Indeed, Cladaras et al. (5) performed hydrophobic moment calculations on apoB, as previously done by DeLoof et al. (82) on apoE, the other well-characterized ligand of the LDL receptor (83), and this pointed to the presence of several possible interacting regions enriched in positively charged residues. The top candidate of this analysis, sometimes called site B, had much in common with the receptor-binding domain of apoE, and experiments with a synthetic peptide (apoB 3,345–3,381) (38) showed the importance of this region in receptor binding and internalization of LDL particles. This did not, however, exclude the importance and/or participation of other domains.

Additional evidence came from experiments with monoclonal antibodies. Unlike the region between residues 2,980 and 3,780, the rest of the protein remained accessible for antibodies while LDL was bound to its receptor (84). Subsequently, Law and Scott (85) compared the sequences of apoB in seven species, and concluded that site B (3,359–3,367) is the primary site involved in receptor interaction.

Truncation mutants of apoB also provide information, as apoB-67 (the amino-terminal 67% of the protein) did not interact with the LDL receptor (86), but apoB-75 (the protein up to residue 3,387) was fully active (87). One important recent report further validates this and provides additional insights into the modulation of the receptor-binding domain as it becomes available for interaction during metabolic conversion of VLDL to LDL. Boren et al. (88) convincingly showed through site-directed mutagenesis that site B is indeed the domain interacting with the receptor. In addition, these experiments showed that the arginine in position 3,500, when mutated to a glutamine, changes the conformation of the C-terminal tail, reducing receptor binding and explaining the molecular basis of the genetic disorder, familial defective apoB-100 (89). The same mutation in apoB devoid of its 20% C-terminal domain did not disrupt receptor binding, but dramatically increased the binding of VLDL, thereby initiating our understanding of the conformational changes in apoB that modulate its metabolic fate.

Although the preeminence of site B in receptor binding with the LDL receptor is now clear, a recent report suggested that charged clusters might be important in the catabolism of truncated apoB mutants. ApoB-70.5 (truncating at residue 3,196) contains site A (3,129–3,151), but not site B; it does not interact with the LDL receptor, but it interacts with LRP-2, the megalin receptor (90). The latter observation seems to be an exception, as unmodified apoB has not been described as the regular mediator of the interaction with other members of the LDL-receptor gene family including the chylomicron remnant receptor or the VLDL receptor [for a review, see ref. (91)].

In addition to LDL-receptor binding, apoB is known to interact with proteoglycans, a process also relevant in the pathogenesis of atherosclerosis (92). Heparin has been used as a model for this interaction, and several heparin-binding domains of apoB have been localized (93, 94) Synthetic peptide work in an in vivo atherosclerosis model demonstrated the importance of a charged cluster other than site B (i.e., residues 1,000–1,016) (95), and more recent work (96) showed the potential for other, also positively charged peptides. In addition, Goldberg et al. (97) showed that apoB-48 lacking site B was capable of binding proteoglycans, explaining why apoB-48-containing lipoproteins may be equally atherogenic. The work of Boren et al. (98) on apoB-100, however, points strongly toward site B as the primary binding site for these interactions with full-length apoB. In addition, they showed that mutants defective in proteoglycan binding could retain their LDL-receptor affinity. Together, these experiments again suggest that apoB is capable of major conformational changes with important metabolic consequences.

The repercussion of these interactions with proteoglycans is the retention of lipoproteins in the arterial wall, making it possible for the apoB-containing lipoprotein particles to become modified [for a review of the different mechanisms, see ref. (92)]. These modified lipoproteins are avidly taken up by the cell though different receptors, resulting in foam cell formation. The quantitative importance of these different mechanisms, the molecular detail of these receptor interactions, and the apoB domains involved remain largely unexplored.

New computer analyses

In this section, we analyze the sequence and structural homology of the putative LDL-receptor binding region within the amphipathic β-strand domain, β_2. These analyses provide insights into mechanisms of receptor binding that both complement and supplement previously published results.

Figure 6 is a LOCATE analysis (35, 44) of residues 2,501–4,100 from human apoB-100, showing the predicted distribution of amphipathic β strands, positively charged amphipathic α-helices, prolines, prolines plus valines, and cysteines. Three long well-defined positively charged amphipathic α-helices, residues 3,129–3,151, 3,170–3,208, and 3,347–4,479, are identified. The first

and last of these helices correspond approximately to site A and site B, respectively, as previously described (4, 5, 38, 81, 82). The middle helix, termed site C, has not been described previously.

Three proline-rich domains (prd) previously described (32, 99) are clearly delineated in Fig. 6 between residues 2,551–2,740 (prd1), 3,216–3,291 (prd2), and 3,687–3,865 (prd3). These domains, possibly representing partial gene duplications (32), are also rich in valine (Fig. 6). As previously noted (34), prd2 separates site A from site B; this domain also separates site C from site B.

Three lines of evidence suggest that the prd2 domain forms a condensed protein structure unassociated with the lipid surface of LDL (condensed domain). First, as defined by the disulfide bond between the cysteines at residues 3,167 and 3,297 (Fig. 6), prd2 (as well as site C) is part of a local loop in the structure of apoB-100 on the LDL particle. Because this disulfide bond is absent in apoB from all other species in which sequence information is available (44), the loop encompassing prd2 and site C seems to be independent of disulfide bond formation. Second, a study of apoB peptides released from the surface of native LDL (99) concluded that the prd2 domain is surface exposed and free of interaction with lipid; 4 of the 11 peptides isolated in this study were from the prd2 domain. Finally, the pdr2 domain, site C, and both cysteine residue positions are missing in the sequence of salmon apoB-100 [ref. (100), Fig. 6, and **Fig. 7**], yet fish LDL binds to the human fibroblast LDL receptor with comparable affinity to human LDL (101).

The other two prd (prd1 and prd3) also appear to form condensed domains on the surface of LDL. The study by Forgez et al. (99) found that peptides from both prd1 and prd3 were also released by trypsin treatment of native LDL. Further, the prd3 (and possibly the prd1) domain, like the prd2 domain, is missing in the sequence of salmon apoB-100 (Fig. 7).

Figure 8 (left panel) is a plot of the positively charged amphipathic α-helices identified by LOCATE between residues 3,001 and 3,500 in apoB-100 from 10 species of vertebrates (human, monkey, pig, mouse, rat, hamster, rabbit, chicken, frog, and salmon). As can be seen, site A is present as a well-conserved amphipathic α-helix located between residues 3,129 and 3,151 in mammals, but is missing in birds, amphibians, and fish. These results support the view that site A is not the primary LDL-receptor binding site. The presence of site A in mammals only is an intriguing observation with uncertain significance.

On the other hand, site B is present as one or two considerably less well-conserved amphipathic α-helices be-
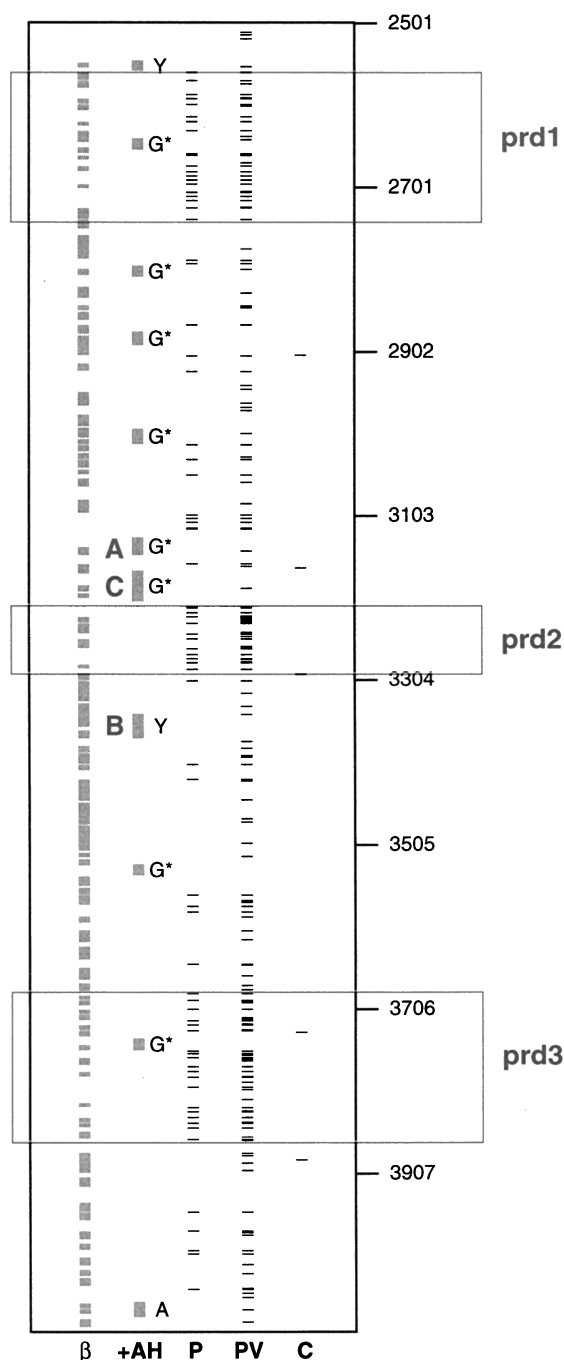
Fig. 6. Mapping of amphipathic motifs, proline-rich clusters, and cysteine residues to the β_2 domain of apoB-100. Amphipathic motifs and the positions of proline, proline plus valine, and cysteine residues identified by the program composite LOCATE in the amino acid sequence of residues 2,501–4,100 of apoB-100 are plotted within the black box. The locations of amphipathic β strands are represented by gray bars, labeled β (left column), positively charged amphipathic α-helices are represented by gray bars labeled +AH (left middle column), proline residues by black lines, labeled P (middle column), proline plus valine residues by black lines, labeled PV (right middle column), and cysteine residues by black lines, labeled C (right column). Parameters used for location of amphipathic β strands were length ≥6 residues, hydrophobic moment ≥1, proline termination and a total hydrophobicity of the nonpolar face ≥5 kcals/mol. Parameters used for location of positively charged amphipathic α-helices were length ≥10 residues, a Λα (calculated lipid affinity) ≥7 kcals/mol selected using helix termination rules that ignore the presence of hydrophobic residues on the polar face, and a net positive charge ≥3. For each amphipathic α-helix plot, the black capital letter to the right of each identified amphipathic helix indicates its amphipathic α-helix class. Sites A, B, and C are indicated by capital letters to the left of the appropriate helix. The three prd are denoted by boxes.
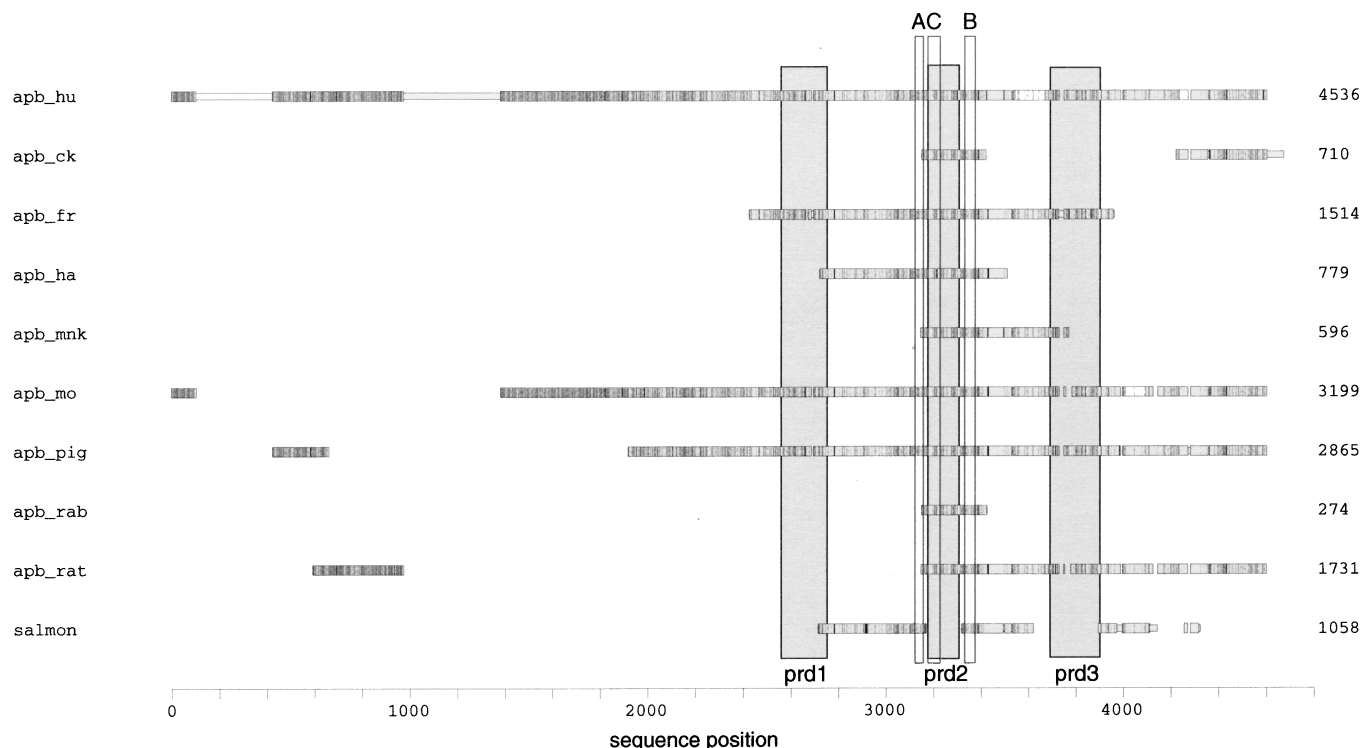
Fig. 7. Alignment of the complete human apoB-100 sequence and determination of sequence homology with partial apoB-100 sequences from six mammals, one bird, one amphibian, and one fish. Alignment and sequence homology analyses were performed with MACAW multiple sequence alignment program (146, 147). Partial sequences of apoB-100 from nine species of vertebrates (chicken, frog, hamster, monkey, mouse, pig, rabbit, rat, and salmon) were obtained in the FASTA format from ENTREZ. This figure is a schematic of the results of the MACAW analysis. Sequences available for the apoB-100 of each vertebrate species are denoted by bars. The narrower white bars represent sequences in which there is no overlap or homology. The thicker bars, with shading denoting degree of similarity, denote regions of linked homology blocks. Gaps represent regions of sequence in which insertions have occurred in other sequences. The three prd are represented by shaded boxes. The approximate location of sites A, B, and C are indicated by narrow open boxes.

tween residues 3,345 and 3,377–3,404 in all species examined including fish. These results are compatible with site B being the primary LDL-receptor binding site, although its interspecies conservation is not as strong as previously suggested by Law and Scott (85).

Site C is present and fairly well conserved in all species except salmon in which that portion of the sequence is deleted (Fig. 8, black bar, right panel), and in hamster in which there is an additional positively charged amphipathic α-helix located between site B and the prd2 domain that is not present in other species. The possible function of site C is unknown.

Figure 8 (right panel) is a LOCATE plot of all proline residues between residues 3,001 and 3,500 in apoB-100 from the 10 species of vertebrates whose sequences are available. The location of the disulfide bond present in human apoB-100 is also shown. As can be seen, a striking clustering of mostly conserved proline residues is present between residues 3,216 and 3,291 in mammals, birds, and amphibians; a cluster that is deleted in salmon (Fig. 8, black bar, right panel). Interestingly, the homologous residue positions of the two cysteines forming the bond are framed on their N- and C-terminal sides by isolated prolines that just fall within the salmon deletion (Fig. 8, black bar, right panel).

We postulate that all three prd (prd1, prd2, prd3) form condensed domains, defined as protein folds on the surface of LDL not associated with lipid. Further, we speculate that these regions may be related to apoB-100 structural changes during the conversion from VLDL to LDL.

LDL STRUCTURE

Published LDL models

It has been generally assumed that LDL is a spheroidal particle approximately 200 Å in diameter that contains a cholesteryl ester-rich core surrounded by a phospholipid-rich shell (60). The issue addressed in this section is the molecular organization of the apoB-100 molecule on the phospholipid-rich surface of the LDL particle and the implications of this organization for overall particle structure and function.

Schumaker and colleagues have painstakingly mapped the positions of 11 anti-apoB monoclonal antibodies onto the surface of human LDL by electron microscopy (102). The first 89% of apoB-100 was modeled as a thick ribbon that wraps once around the LDL, completing the encirclement by approximately amino acid residue 4,050 (the junction of the β_2 and the α_3 domains). The thickness of
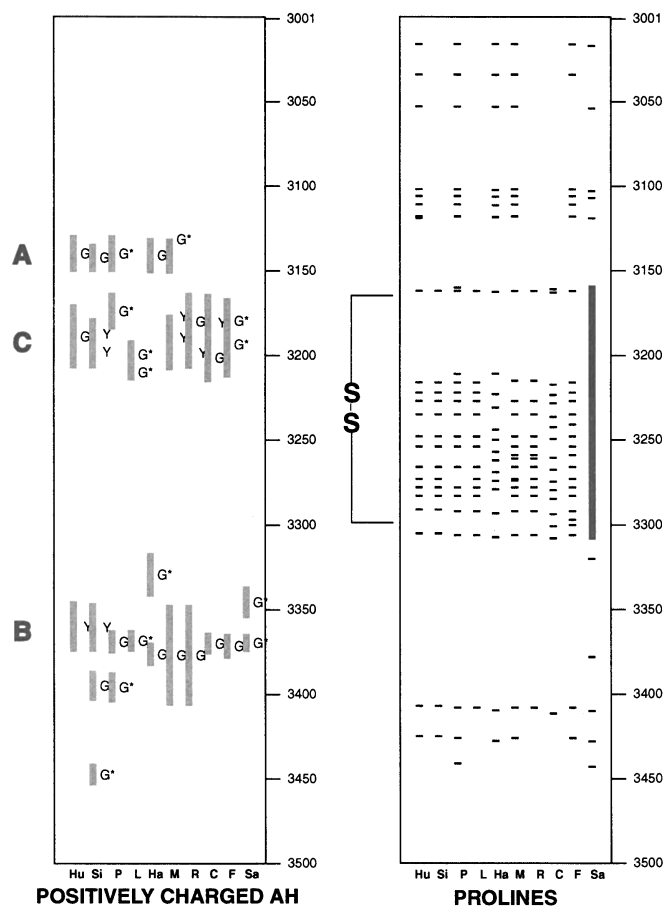
Fig. 8. Mapping of positively charged amphipathic helices and proline-rich clusters to the β_2 domain of apoB-100. Left panel: this is a plot of the positively charged amphipathic α-helices identified by LOCATE between residues 3,001–3,500 in apoB-100 from 10 species of vertebrates (human, monkey, pig, mouse, rat, hamster, rabbit, chicken, frog, and salmon). Parameters used for location of positively charged amphipathic α-helices were length $\geqslant$10 residues, a $\Lambda\alpha$ (calculated lipid affinity) $\geqslant$5 kcals/mol selected using helix termination rules that ignore the presence of hydrophobic residues on the polar face, and a net positive charge $\geqslant$3. Sites A, B, and C are denoted with capital letters. Right panel: this is a LOCATE plot of all proline residues between residues 3,001–3,500 in apoB-100 from the 10 species of vertebrates whose sequences are available. The location of the disulfide bond present in human apoB-100 is also shown. The deleted sequence in salmon is indicated by the black bar.

the ribbon was proposed to be approximately 20 Å, sufficient to penetrate the monolayer and to make contact with the core. They proposed a kink in the ribbon beginning almost halfway along its length at approximately apoB-48 (the start of the α_2 domain). The C-terminal 11% of apoB (the α_3 domain) was termed a "bow," an elongated structure of about 480 residues beginning at residue 4,050, stretching back into one hemisphere, and then crossing the ribbon between residues 3,000 and 3,500 into the other hemisphere.

The most complete modeling of the lipid and protein components of LDL subclasses is an elegant study by McNamara et al. (21). These authors combined the use of nondenaturing gradient gel electrophoresis and ultracen-

trifugation with calculations of the number of molecules of each lipid and protein component of eight distinct LDL subclasses from 66 subjects to derive detailed compositional models for each subclass. Their conclusion was that differences in LDL subclasses involve both changes in lipid composition and conformational changes in apoB-100. In particular, they concluded that apoB-100 progressively unfolds to cover an increasing area of the LDL particle surface as LDL subclasses decrease in size.

Several models for LDL have been suggested from studies using low angle X-ray scattering (13, 14, 103). Most of the models were based upon an oil droplet or microemulsion model containing a predominantly cholesteryl ester lipid core (104). Relevant to the cholesteryl ester core model, a broad phase transition in LDL was observed by differential scanning calorimetry and X-ray and neutron solution scattering at a temperature in the range of 19–32°C (12, 104–111). The transition was associated with a smectic-to-disorder phase change of cholesterol esters within the particles. Below the transition temperature, in the smectic phase, a $1/36$ Å^{-1} reflection was observed in X-ray solution-scattering experiments (12).

van Antwerpen and collaborators (112–114) reported images of LDL analyzed in a vitrified frozen-hydrated condition without chemical fixation or any form of staining (cryoelectron microscopy). Based upon these studies, it was concluded that the overall shape of human LDL was discoidal (**Fig. 9A**). The observed LDL discs were reported to have a diameter of 214 $\pm$ 13 Å and a height of 121 $\pm$ 11 Å. These authors concluded that apoB-100 appeared to form two ring-shaped structures around the perimeter of the LDL disk.

Spin and Atkinson (115) also reported images of LDL in vitreous ice using electron cryomicroscopy (at approximately 30-Å resolution). As shown in Fig. 9B, LDL appeared in their study to be a quasi-spherical particle approximately 220–240 Å in diameter, with a region of low density surrounded by a ring (in projection) of high density believed to represent apoB-100. The ring was noted to be composed of four or five large regions of high density material, presumably protein superdomains, connected by regions of lower density. Some images were egg shaped and contained a pointed end; the pointed end (arrow in Fig. 9B) was postulated to represent the N-terminal globular region (the $\beta\alpha_1$ domain) of apoB. These authors also observed disc-shaped structures similar to those seen by van Antwerpen and collaborators (112–114), but considered these objects artifacts.

In a third article using electron cryomicroscopy, a three-dimensional structure of LDL particles at 27-Å resolution was reported by Orlova et al. (116). Multivariate statistical and cluster analyses were used to identify a subset of structurally homogeneous LDL particles from a larger pool of particles with heterogeneous sizes and features. Angular reconstitution was then used to develop a three-dimensional model from a subset of 2,600 particles in 129 classes. Figure 9C is a three-dimensional map of the ellipsoid LDL structure with dimensions of 250 × 210 × 175 Å (116). Two features of this model are especially note-

worthy. First, a knob-shaped electron-dense object appears on the surface of the model (red arrow), with dimensions (35–45 Å) that approximate the βC globular domain of lipovitellin. Further, the knob contains a central cavity (10–20 Å in diameter) that is similar to the cavity found in the βC domain (red arrow). Second, the core of the model contains three major higher density planar layers approximately 35 Å apart (Fig. 9C, black arrow). The authors suggested that these layers might represent cholesteryl ester in the smectic phase. Because LDL undergoes a smectic-to-disordered phase transition in the range of 19–32°C (12, 104–111), both the flattening of the LDL model and its core organization may be artifacts of the cryogenic temperatures. This model presumably is related to the discoidal structures reported by van Antwerpen and collaborators (112–114).

Two groups have been able to crystallize LDL (117, 118). The second of these groups (119) recently determined a preliminary X-ray crystallographic model for LDL-2 at 27-Å resolution. Figure 9D shows a stereo view of their model (M. Baumstark, personal communication). Interestingly, this model appears to show the two principal features of the Orlova et al. (116) model: a surface knob with the dimensions of the βC globular domain of lipovitellin (red arrow, Fig. 9D) and a planar multilamellar core (black arrow, Fig. 9D). The diffraction data was collected at cryogenic temperatures.

## New analysis of published data

The constraint in both the Chatterton et al. (102) and the McNamara et al. (21) studies was a lack of knowledge at that time of the pentapartite organization of apoB-100 (35, 44). We have used the information contained in the pentapartite domain structure of apoB-100 (35, 44) shown in Fig. 2 in a re-analysis of the organization of apoB-100 on the surface of the eight so-well-characterized LDL subclasses of McNamara et al. (21). Their model used the following two assumptions:

First, McNamara et al. (21) assumed that both phospholipid *and* free cholesterol are in contact with the core lipid, and they applied surface pressure assumptions directly to the core surface in order to determine the fraction of the core surface covered by these polar lipids. In our calculations, we assumed that phospholipid and free cholesterol affect the packing of the polar lipids at the aqueous surface of the LDL particles, but that only the fatty acyl chains of the phospholipid make contact with the lipid core.

Second, they assumed that the core lipids of LDL are arranged in a regular spheroidal shape that is in direct contact over a fraction of its total surface with a 20-Å thick section of apoB-100 (21). Our model assumed that only that portion of apoB-100 that forms amphipathic β sheets (35, 44) is in direct contact with the lipid core. Further, because no protein structural motif is known to form a sta-
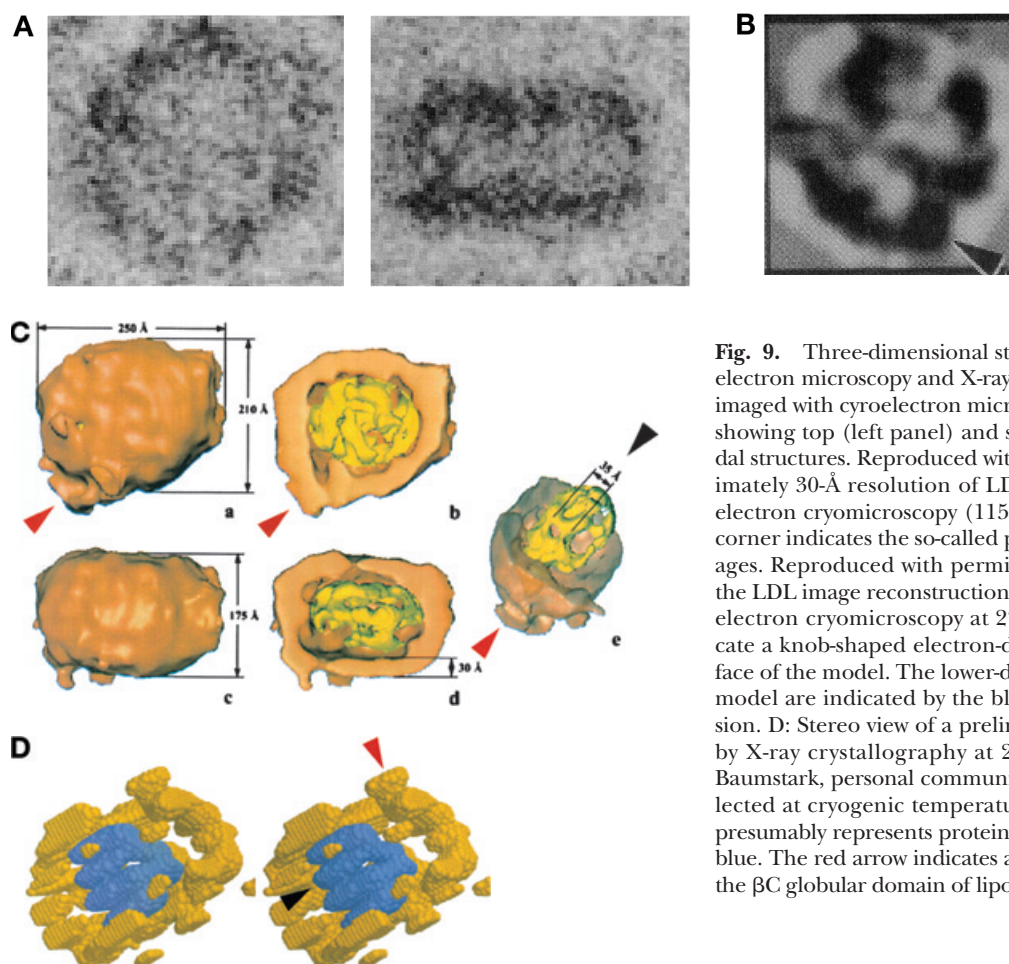
Fig. 9. Three-dimensional structure determined for LDL by cryo-electron microscopy and X-ray crystallography. A: Two views of LDL imaged with cyroelectron microscopy by van Antwerpen et al. (114) showing top (left panel) and side (right panel) views of the discoidal structures. Reproduced with permission. B: An image at approximately 30-Å resolution of LDL in vitreous ice determined using electron cryomicroscopy (115). The arrow in the lower right-hand corner indicates the so-called pointed end found in many of the images. Reproduced with permission. C: Three-dimensional map of the LDL image reconstruction reported by Orlova et al. (116) using electron cryomicroscopy at 27-Å resolution. The red arrows indicate a knob-shaped electron-dense object that appears on the surface of the model. The lower-density planar layers in the core of the model are indicated by the black arrow. Reproduced with permission. D: Stereo view of a preliminary model for LDL-2 determined by X-ray crystallography at 27-Å resolution [(118, 119) and M. Baumstark, personal communication]. The diffraction data was collected at cryogenic temperatures. The electron-dense region that presumably represents protein is indicated in gold; the core lipid in blue. The red arrow indicates a surface knob with the dimensions of the βC globular domain of lipovitellin. Reproduced with permission.
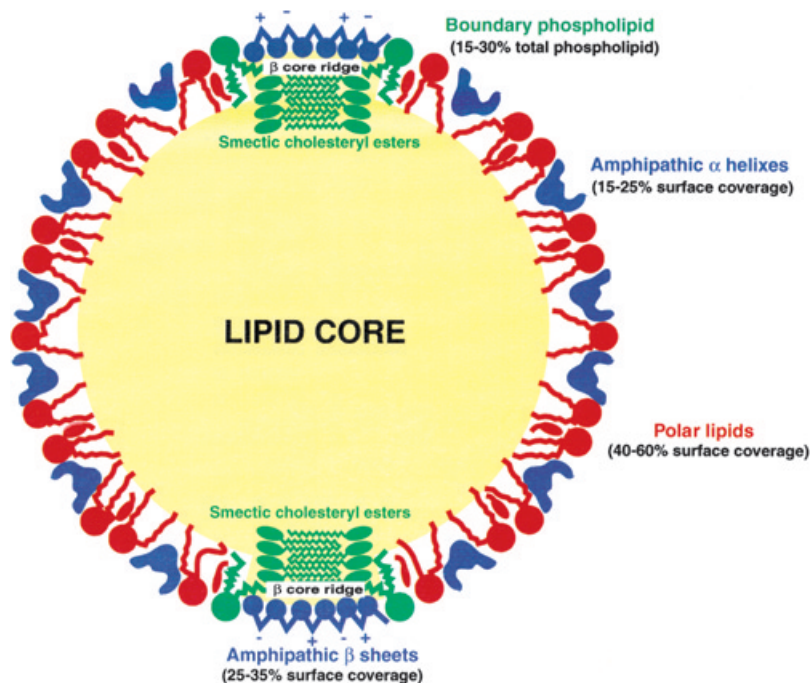
Fig. 10. Diagrammatic cross-sectional model of the proposed amphipathic β sheet/lipid-core ridge model for LDL shown approximately to scale. Color code: blue, protein; red, unrestricted surface phospholipid plus unesterified cholesterol; green, boundary surface phospholipid and smectic cholesteryl ester phases; yellow, cholesteryl ester-rich core.

ble structure that extends 20 Å into a lipid monolayer, we assumed that the core lipid in contact with the amphipathic β sheets forms ridges that extend to within 7 Å of the LDL aqueous surface (**Fig. 10**). We further assumed that amphipathic helices from the α domains of apoB-100 (35, 44) act much like free cholesterol to increase the packing density of the polar lipids at the aqueous surface of the LDL particles.

Six additional assumptions were used to develop our model: first, we assumed, as first suggested by Small and Atkinson [(54) and personal communication], that the individual β strands of the β_1 and β_2 domains of apoB-100 form continuous β sheets. Further, the number (Nβ) and the mean residue length (Lβ) of lipid-associating amphipathic β strands [predominantly located in the β domains of apoB-100 as defined previously (35, 44)] can be determined using the computer program LOCATE (35, 44, 120, 121). From this, we calculated that for the β_1 sheet, Nβ = 81 and Lβ = 12.2 and, assuming condensed loops at the three prd of β_2, Nβ = 63 and Lβ = 12.0 for β_2.

Second, each amphipathic β sheet has a mean thickness of approximately 7 Å (determined by molecular modeling; results not shown) and, thus, exerts its maximal effect on surface area at a depth of 3.5 Å from the aqueous surface of each LDL subclass.

Third, the surface area (SA) per polar lipid (i.e., phospholipid + free cholesterol) has been calculated for each of the individual LDL subclasses by McNamara et al. (21), and varies from 51–55 Å².

Fourth, amphipathic helices of apoB-100 are postulated to be evolutionarily selected for a wide range of lipid affinities (Λα) from a large number with low lipid affinity or greater to only a few with extremely high Λα. The number and mean residue length of lipid-associating amphipathic α-helices for a given lower limit of Λα can be determined

by the computer program; the higher the Λα cutoff, the fewer the amphipathic helices.

Fifth, each lipid-associated amphipathic α-helix exerts its maximal effect on surface pressure at a depth of 7 Å from the aqueous surface of each LDL subclass (122) (see footnote to **Table 1**).

Sixth, the radius (rc_i) and surface area (SAc_i) of the effective core (core minus the volume of the β core ridges) for each LDL subclass, i, were calculated assuming that phospholipid monolayers containing amphipathic helices are 23 Å thick (122). Thus $rc_i = (r_{LDL_i} - 23)$ and $SAc_i = [4\pi \times (r_{LDL_i} - 23)^2]$.

Table 1 contains calculations of the fractional surface area coverage by polar lipid, amphipathic β sheets, and amphipathic α-helices as a function of LDL subclass. The equations used are included in a footnote to the table. As first pointed out by McNamara et al. (21), these results indicate that the fractional area occupied by surface lipids decreases with decreasing LDL subclass size, whereas the fractional surface estimated to be covered by amphipathic α-helices increases with decreasing size.

The total surface area in Å² covered by amphipathic α-helices can then be calculated as a function of LDL subclass; the results are shown in Table 1. Compatible with the conclusion by McNamara et al. (21), these calculations indicate that the total surface area covered by amphipathic α-helices increases as LDL subclasses decrease in size.

Determination of the approximate number of amphipathic α-helices associated with each LDL subclass can be made from the surface area data. These calculations involve using the computer program LOCATE to construct a table (**Table 2**) of the number of lipid-associating amphipathic α-helices and the LDL surface area that would be occupied by these helices (see footnote to Table 2) as a function of lipid affinity less than a given Λα. Then, the

TABLE 1. LDL surface composition calculated from the pentapartite model for apoB-100

Calculated Properties	LDL Subclasses							
	1	2	3	4	5	6	7	8
Surface fraction covered by								
Polar lipids[a]	0.572	0.574	0.551	0.510	0.484	0.468	0.446	0.378
Amphipathic β sheets[b]	0.266	0.275	0.276	0.287	0.296	0.303	0.307	0.356
Amphipathic AH[c]	0.162	0.151	0.174	0.203	0.220	0.229	0.247	0.266
Total surface area (A²) of lipid-associated AH	18,338	16,399	18,866	21,205	22,198	22,579	24,018	22,206
Number of lipid-associated AH	51 ± 8	45 ± 8	53 ± 8	62 ± 9	65 ± 9	67 ± 9	71 ± 9	65 ± 9
PL molecules per lipid-associated AH	16.0	17.7	14.5	11.3	10.2	9.3	8.4	6.8
Surface area (A²) per PL molecule of								
Fatty acyl chains at lipid core[d]	70.1	68.0	70.2	72.2	72.7	74.2	75.6	78.2
Headgroups at aqueous surface[e]	57.7	57.5	57.6	58.0	58.4	58.4	58.8	59.5
Mole fraction of boundary PL[f]	0.165	0.170	0.177	0.197	0.211	0.224	0.236	0.320

Abbreviations: AH, α-helices; PL; phospholipid.

[a] The fraction of the aqueous surface area (SA) of each LDL subclass (i) covered by the polar lipid (L) is calculated by the equation $[SA_{Li}] = (SA/L_i \times N_{Li})/[4\pi \times (r_{LDLi} - 7)^2]$, where N_{Li} = total number of polar lipid molecules per LDL subclass particle.

[b] The total surface area in A² occupied by the continuous amphipathic β sheet of each β domain (i) is calculated by the equation $SA\beta_i = (N\beta_i \times 4.7 \text{ Å}) \times (L\beta_i \times 3.4 \text{ Å}^2)$, where 4.7 Å is the distance between strands, 3.4 Å is the distance along each β strand per residue, and Nβ is the number and Lβ is the mean residue length of lipid-associating amphipathic β strands. From this, we calculate $SA\beta_1 = 18,380$ Å² and $SA\beta_2 = 13,893$ Å². The fraction of the aqueous surface of each LDL subclass (i) covered by the amphipathic β sheets of the β_1 plus β_2 domains is calculated by the equation $[SA\beta] = (SA\beta_1 + SA\beta_2)/[4\pi \times (r_{LDLi} - 3.5)^2]$.

[c] The fraction of the aqueous surface area of each LDL subclass (i) covered by amphipathic AH is calculated by the equation $[SA_{AHi}] = 1 - [SA_{Li}] - [SA\beta_i]$.

[d] Areas for the phospholipid fatty acyl chains at the lipid core (C) of each LDL subclass (i) were calculated by the equation $SA_{Ci}/PL_i = (SA_{Ci} \times [SA_{Li}])/N_{PLi}$, where N_{PLi} = total number of phospholipid molecules for a given LDL subclass (i).

[e] Areas for the phospholipid headgroups at the aqueous surface were calculated by the method of Ibdah, Lund-Katz, and Phillips (134) applied to the surface area per polar lipid taken from McNamara et al (21).

[f] From the equations in footnote b, the β_1 sheet is calculated to have a length of 381 Å; the β_2 sheet, a length of 296 Å. Thus, the lateral perimeter (P_L) is $P_L = (381 \text{ Å} \times 2) + (296 \text{ Å} \times 2) = 1,354$ Å. The effective diameter of phospholipid in each LDL subclass ($_ed_{PL}$) is calculated as follows: SA_L (surface area of total lipid) = SA/L [surface area per lipid taken from McNamara et al. [(21)] $\times N_L$ [total surface lipid taken from McNamara et al. (21)]. Then, eSA/PL (effective surface area per phospholipid molecule) = $SA_L \times N_{PL}$ [total surface phospholipid taken from McNamara et al. (22)]. From eSA/PL, $_ed_{PL}$ can be calculated. For example, for LDL-1, $_ed_{PL}$ is 10.03 Å. Thus, the mole fraction boundary phospholipid $[PL_b]$ is $[PL_b] = (P_L/_ed_{PL})/N_{PL}$. For LDL-1, $[PL_b] = 0.165$.

LDL subclass surface area data is interpolated onto the table. The number of lipid-associated amphipathic helices (AH) and the number of phospholipid (PL) molecules per lipid-associated amphipathic helix (PL/AH) calculated for each LDL subclass by this interpolation are shown in Table 1. The smallest subclass, LDL-8, has the lowest PL/AH ratio (6.8), with a ±10% range of 6.3 to 8.9. This ratio suggests that the amphipathic helices of LDL-8 are separated, on average, by one layer of phospholipid (see later discussion), although extensive helix-helix interaction is another possibility.

Another interesting calculation is to determine for each LDL subclass the surface area per phospholipid molecule for the fatty acyl chains at the lipid core, and the head-

groups at the aqueous surface (Table 1). To put the resulting calculation in perspective, phospholipid molecules of the highly curved outer monolayers of small unilamellar vesicles (particles that are close to the diameter of LDL), in the absence of cholesterol, have an area per headgroup of approximately 90 Å² (123) compared with 72 Å² for more planar monolayers. Further, small unilamellar vesicles have a headgroup/fatty acyl chain methyl area ratio of approximately 1.7 (123).

It has been shown that smaller phospholipid vesicles have a much greater affinity for apoA-I (124) or model amphipathic helical peptides (V. K. Mishra and J. P. Segrest, unpublished observations) than larger vesicles or multilamellar vesicles. This difference in affinity was ex-

TABLE 2. Table for interpolation of the number of surface-associated amphipathic α-helices of different LDL subclasses

Properties	Λα															
	8.5	≥9	≥10	≥11	≥12	>13	13.1	≥14	14.6	≥15	≥16	≥17	≥18	≥19	19.1	≥20
Total surface area (A²) covered[a]	27,846	23,963	19,278	17,280	15,240	11,310	—	9,648	—	7,838	7,395	6,390	4,680	3,708	—	3,015
Number	84	71	54	48	40	29	—	24	—	19	17	15	10	8	—	6
Peptide exclusion pressure (dyn/cm)[b]	30	—	—	—	—	—	38	—	40	—	—	—	—	—	45	—

[a] The total surface area in A² covered by amphipathic helixes for each Λα cutoff is calculated by the equation $SA_{AH\Lambda i} = N_{\Lambda i} \times (L_{\Lambda i} \times 15 \text{ Å}^2)$, where 15 Å² is the surface area per residue for amphipathic α-helixes associated with lipid monolayers (134, 144).

[b] These represent four amphipathic helical peptides with measured surface exclusion pressures of 30, 38, 40 and 45 dyn/cm (2data not shown) for which Λα calculations were made.

plained by Wetterau and Jonas (124) as resulting from the increasing bilayer curvature of smaller vesicles that increases the surface area per headgroup of the PC molecules in the outer monolayer of the bilayer and, thus, facilitates penetration by amphipathic helices. Smaller phospholipid vesicles thus have lower surface pressures than larger phospholipid vesicles. Therefore, in the absence of protein, highly curved LDL particles would be expected to have very low surface pressures but, in fact, have high surface pressures (21); free cholesterol can account for some, but not all, of the increased surface pressure.

Illustrating the quite considerable surface pressure exerted on the phospholipid monolayer of LDL by the combination of free cholesterol, amphipathic β sheets, and the amphipathic helices of apoB-100 from Table 1, the ratios of the surface area of the headgroups to that of the fatty acyl chains for the eight LDL subclasses are reversed from the 1.7 of the outer phospholipids of small unilamellar vesicles to 0.846 and 0.770 for LDL-2 and LDL-8, respectively. This suggests that the fatty acyl chains of phospholipid molecules at the core of LDL are more mobile than the headgroups at the aqueous surface or, more likely, there is interdigitation of core lipids such as the fatty acyl chain of the cholesteryl esters into the phospholipid/core interface (125–127).

Five tests of the plausibility of the pentapartite model developed here for LDL were made. First, studies using both ^{31}P-NMR (128) and ^{1}H-NMR (129) indicated that approximately 20% of the phospholipid in LDL was immobile. Further, because phospholipid is not immobilized in HDL (130, 131), immobilization must not be the result of phospholipid contact with the edges of the amphipathic helices of apoB-100 but, rather, must be the result of phospholipid contact with the perimeter of the amphipathic β sheets (so-called boundary lipid). Calculation of the approximate dimensions of the lateral perimeter of the amphipathic β sheets of the $β_1$ and $β_2$ domains of apoB-100 (see Table 1 footnote) allows an estimate of the mole fraction of phospholipid of each LDL subclass in contact with this motif (Table 1). The results are compatible with immobilization of approximately 20% of the phospholipid in the most common of the LDL subclasses (LDL-3 to LDL-5) by contact with the edge of the amphipathic β-sheet motifs of apoB-100.

More recent studies by Murphy et al. (132, 133) using 600 MHz ^{1}H-NMR showed an average immobilization of 24% of the phospholipid in LDL from nine individuals, with a measured range of 16% to 30%. Although the differences in LDL subclasses among the nine individuals studied has not yet been reported, the range in immobilized phospholipid reported by Murphy et al. (132, 133) is strikingly similar, respectively, to the boundary lipid range calculated in Table 1 for LDL-1 to LDL-8.

As a second test, the calculated and 10% confidence interval minimum Λα (9.0 and 8.6, respectively) determined for LDL-7 (interpolate the results in Table 1 onto Table 2) are greater than the Λα of 8.5 calculated for a model peptide with a measured surface pressure of 30 dyn/cm, the minimum surface pressure estimated for LDL

(21, 134). Further, the predicted surface area occupied by lipid-associated amphipathic helices for the eight LDL subclasses indicates a particle surface pressure that varies from ≥30 dyn/cm for LDL-7 to >38 dyn/cm for LDL-2. These surface pressures are reasonable and compatible with the known surface properties of LDL.

As a third test, it can be shown using molecular modeling on a graphics workstation that amphipathic helices that are 22–29 residues in length embed in phospholipid to form a single layer of phospholipid molecules between each amphipathic helix will have a PL/AH ratio of approximately 4/6. Thus, a lower 10% confidence limit of 5.9 for the PL/AH ratio of the smallest LDL subclass (Table 1) is not unreasonable

A fourth test is related to the dimensions of apoB, as determined by Schumaker and his colleagues on the basis of the mapping of monoclonal antibodies to the surface of LDL particles (60, 102). A 200-Å diameter LDL particle has a circumference of approximately 630 Å. A recent electron cyromicroscopy study by Gantz, Walsh, and Small (53) reported that sodium deoxycholate-solubilized apoB-100 is a flexible molecule approximately 650 Å in length. LOCATE analysis of the two predicted amphipathic β sheets of apoB-100 suggests a cumulative length of 677 Å (381 Å + 296 Å), close both to the circumference of LDL and to the apoB-100 length suggested by Gantz, Walsh, and Small (53).

Finally, studies on the induced CD of beta-carotene, an intrinsic probe of the neutral lipid core of LDL, showed a reduced transition temperature for cholesteryl esters after trypsin treatment (29), a result interpreted to suggest that the trypsin-accessible regions of apoB may influence the fluidity of the core. A major assumption of the pentapartite model for LDL structure is that the two β-sheet domains of apoB-100, clearly trypsin-releasable (Fig. 2), are in direct contact with the core. The results of Chen, Chapman, and Kane (29) suggest, therefore, that the β-sheet domains of apoB-100 induce the smectic-ordered cholesteryl ester phase (Fig. 10 and **Fig. 11**).

CRITICAL UNRESOLVED ISSUES CONCERNING LDL STRUCTURE

In spite of recent experimental gains discussed in this review, investigators are still a long way from understanding the structure of LDL in detail. There is hope, however. Perhaps a high resolution X-ray crystal structure of LDL is on the horizon. Five years ago, few would have predicted the level of sophistication achieved by the low resolution models of LDL available today. As we noted elsewhere (135), to the extent that lipid-water interfaces inscribe a "signature" in lipid-associating proteins, atomic resolution models for lipoproteins may be achievable by the systematic application of the principle of "lipid signatures." Therefore, in lieu of direct structural determination, the current LDL models may prove useful as templates for further structural analyses. Resolution of at least four critical questions will increase our understanding of LDL structure.
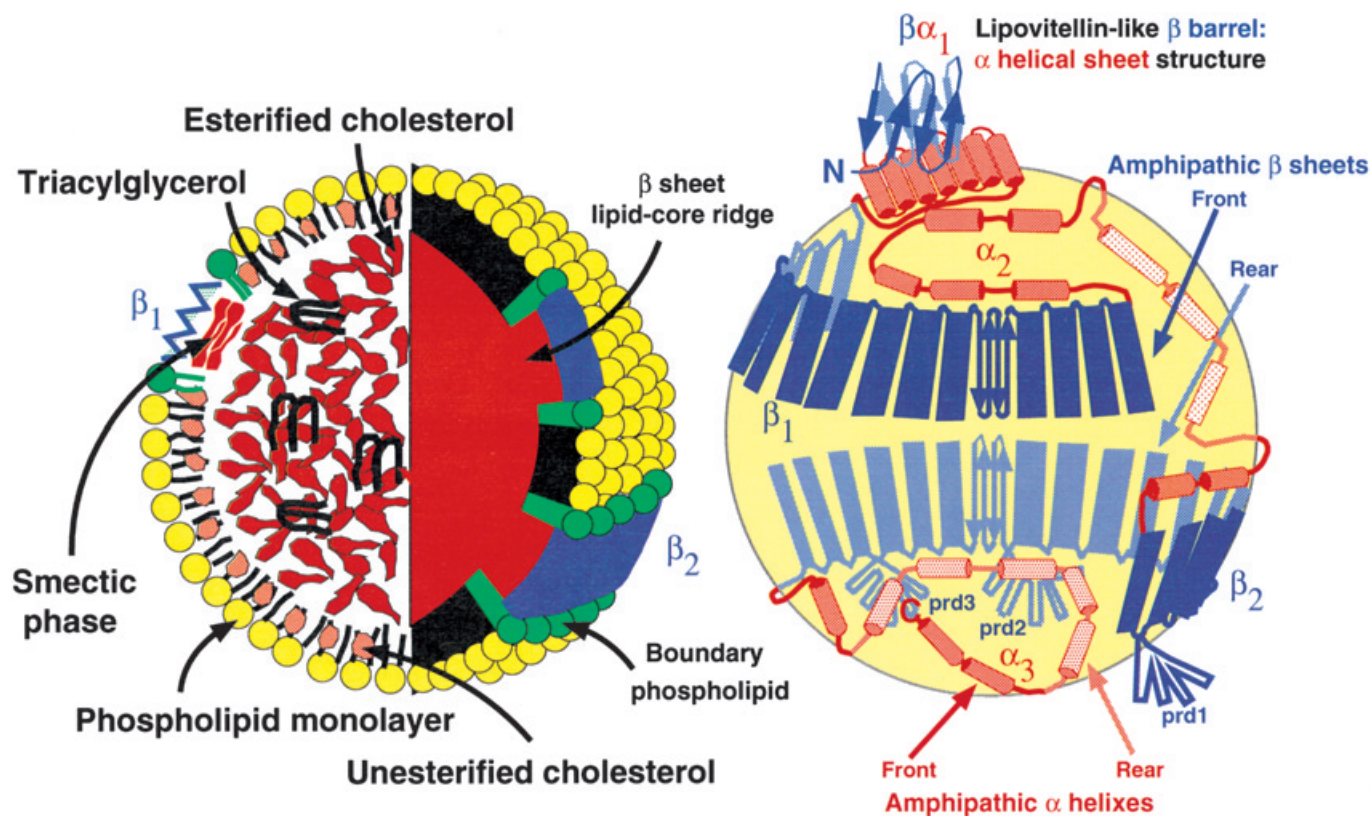
Fig. 11. Schematic diagram of a three-dimensional consensus model for LDL. The left-hand cutaway sphere summarizes the proposed organization of lipid: yellow, surface phospholipid; red, core lipid including amphipathic β sheet-induced lipid-core ridges; green, boundary phospholipid; blue, amphipathic β sheets. The right-hand transparent sphere illustrates the proposed organization of apoB-100 on the LDL particle surface: blue, β structure; red, α-helical structure; darker blue and red, structures on the front of the sphere; lighter blue and red, structures on the back of the sphere. No attempt has been made in this model to illustrate either the bow proposed by Chatterton et al. (102) to be formed by the α_3 domain when it crosses over the β_2 domain near residue 3,500, or the amphipathic α-helical spring between the β_1 and β_2 domains proposed by Hevonoja et al. (127).

One imminent question is whether LDL particles circulating at 37°C are spheroidal in shape, as generally assumed, or are semidiscoidal in shape, as suggested by both cryo-electron microscopy (112–116) and X-ray crystallography (118, 119). Put another way, does a shape change occur in the LDL particle in going from the smectic (liquid crystalline) to the disordered (liquid) phase of the LDL core cholesteryl ester? This thermal transition has been shown to occur in the range of 19–32°C (12, 104–111), and varies depending upon the cholesteryl ester-to-triglyceride ratio (111, 136).

Calculations of LDL surface coverage by amphipathic α-helices depend critically upon knowledge of the true LDL particle shape. The volume of the LDL subclasses can be calculated from compositional data (21). Because a sphere has the smallest surface area/volume ratio possible, flattening of the LDL particle surface at the poles between the amphipathic β_1 and β_2 sheets (converting a spheroidal particle to a semidiscoidal particle) would result in an increase in overall surface area/volume ratio and thus, presumably, an increase in surface area. This surface area increase, in turn, would lead to a shift in the amphipathic α-helical exclusion limits toward lower Λα and lower surface pressures in Table 2, resulting in more surface-associated amphipathic α-helices per LDL particle than calculated in Table 1.

Studies by Baumstark et al. (137) using low angle X-ray diffraction showed that the density profile of LDL at 37°C fitted a particle with spherical (radial) symmetry well, but at 4°C, the same LDL did not fit well to a particle with spheroidal symmetry. Further, they found that LDL at 4°C had slightly larger dimensions than the same LDL at 37°C. Because it is now clear that LDL at 4°C is semidiscoidal (112–116, 118, 119), a reasonable interpretation of the data of Baumstark et al. (137) is that LDL is spheroidal at 37°C. Studies by Parks and Hauser (110) also are compatible with this possibility.

Second, even though there is good reason to assume structural similarity of the $\beta\alpha_1$ domain of apoB to lamprey lipovitellin, the relative low degree of sequence identity, approximately 23% (59), suggests that there might be sufficient differences in folding of some of the structural elements of apoB versus lipovitellin. Further, conversion of the early lipid-poor lipovitellin-like structure of apoB to a true lipoprotein particle during assembly would most likely result in additional changes in apoB conformation (see Fig. 11). Thus, determination of differences between the structures of lamprey lipovitellin and the α_1 domain of apoB represents a second critical problem relating to LDL structure.

A third critical unresolved problem concerns significant uncertainties in the chain trace for the amphipathic β sheets of the β_1 and β_2 domains on the LDL particle surface. None of the existing three-dimensional models for LDL have sufficient resolution to allow localization of the β_1 and β_2 domains without reliable models for chain tracing. Even though an epitope trace for apoB-100 on the LDL surface has been published (102), the usefulness of this trace depends upon whether circulating LDL particles are spheroidal or discoidal in shape and whether the particle, and thus the chain trace, is distorted by dehydration during negative staining (102).

The final unresolved problem relating to LDL structure to be mentioned here is the question of the number, location, and structure of the so-called condensed domains (e.g., prd1, prd2, and prd3, Fig. 11). Because these regions of apoB-100 interrupt the amphipathic β sheets of the β domains, knowledge of their nature is important for future modeling of LDL structure.

DEVELOPMENT OF A CONSENSUS LDL MODEL

Pentapartite organization of apoB-100

Although the precise boundaries of the domains are uncertain, there appears to be a general consensus that apoB-100 is divided into five distinct regions: NH_2-$\beta\alpha_1$-β_1-α_2-β_2-α_3-COOH (Fig. 2). Further, these domains are not entirely homogenous, as there appears to be some admixture of amphipathic α-helices within the β domains, and vice versa [(44) and D. Small, personal communication]. This is especially true of the globular $\beta\alpha_1$ domain (residues 1–1,000) whose heterogeneity in secondary structural elements relates to its structural homology to lamprey lipovitellin (59, 74, 75, 138, 139).

Amphipathic β sheets

The available evidence (53, 102) supports the concept, as suggested originally by Small and Atkinson [(54) and personal communication], that the two β domains form amphipathic β sheets. Less certain is whether each domain forms a continuous amphipathic β sheet broken only by regions of condensed structure such as found in the prd, or whether sheets are discontinuous and perhaps, separated by one or more individual strands. Based upon studies of the interactions of small peptides with water/phospholipid interfaces by Jacobs and White (140), it seems likely that unfavorable energy costs associated with the lack of hydrogen bonds between amphipathic β strands will limit individual strands on lipid surfaces. Further, the creation of neutral lipid core ridges beneath amphipathic β sheets proposed earlier (Fig. 10) would contribute additional favorable free energy not available to individual strands.

Assuming the existence of amphipathic β sheets, is there variability in the length of individual strands within a given sheet? Although LOCATE analyses suggest considerable variability in length of individual amphipathic β strands, the question of variability is unresolved at this time. Also to

be resolved is whether the amphipathic β sheets follow a linear route (e.g., a great circle route around the surface of the LDL particle) or whether the sheets are offset from a great circle route and/or possess kinks (60).

We postulate three functions for amphipathic β strands in apoB beyond determining lipid affinity: first, we suggest that these motifs in the $\beta\alpha_1$ domain participate in lipid accumulation in the co-translationally assembled prenascent TAG-rich lipoprotein particle (the lipid-pocket hypothesis). Second, we suggest a direct contact of the hydrophobic face of amphipathic β sheets with the neutral lipid core of apoB-containing lipoproteins likely playing a role in core lipid organization [e.g., influencing the formation of the 35-Å thick lamellae observed by Orlova et al. (116) and Lunin et al. (119) that probably represent cholesteryl ester organized as planar smectic phases], lipolysis, and/or lipid transfer. Finally, we suggest that the amphipathic β-sheet motifs largely determine LDL particle diameter and, perhaps, participate in the regulation of LDL subclass diameters.

Amphipathic α-helical domains

There is strong evidence that the N-terminal region of apoB is globular. Further, the first 1,000-residue region of apoB, the $\beta\alpha_1$ domain, is clearly homologous to lipovitellin, meaning that the $\beta\alpha_1$ domain of apoB and lipovitellin share similar structural features. In particular, it seems probable that a β barrel structure formed by the N-terminal 200-or-so residues of apoB, related to the βC domain of lipovitellin, is present on the surface of the LDL particle. It also seems likely that the $\beta\alpha_1$ domain of apoB forms a lipovitellin-like proteolipid intermediate containing a lipid pocket during initial assembly of apoB-containing lipoprotein particles. However, most of the $\beta\alpha_1$ domain probably changes its conformation in an as-yet-undefined manner during maturation of the lipovitellin-like proteolipid intermediate to spheroidal apoB-containing particles.

Segrest et al. (35, 44) proposed that the amphipathic helices of the α_1 and α_2 domains represent the reversible lipid-associating domains of apoB-100. The modeling of the pentapartite organization of apoB-100 onto LDL subclass composition and size (the β lipid-core ridge model) supports the general concept that the number of amphipathic helices of apoB-100 associated with the surface lipids of the LDL particle change with particle size and surface pressure. It is reasonable, therefore, to assume that one function of the reversible class A-containing amphipathic helices of the α_2 and α_3 domains of apoB-100 is to modulate the surface pressure decreases that occur as the particle decreases in size during lipoprotein metabolism and lipid exchange. Chylomicrons that remain large and thus, presumably, have a relatively constant surface pressure, would not need the reversible α_2 and α_3 domains; apoB-48 is truncated just before or just at the beginning of the α_2 domain.

On the one hand, the previous suggestion by Segrest et al. (35, 44) that the amphipathic α-helices of the α_2 and α_3 domains of apoB-100 may regulate the discrete quantization of size of the different LDL subclasses is not really supported by the lipid-core ridge model for LDL. An alter-

nate possibility suggested by this model is that the amphipathic β sheets of the β domains control LDL particle size by some form of cinching down of the encircling β belt (60, 102). The mean change in circumference between adjacent LDL subclasses excluding LDL-8 is approximately 9 Å, equal to two amphipathic β strands (or the thickness of one amphipathic helix; see next paragraph). Mechanisms for tightening the encircling β belt might include a dissociation of short stretches of amphipathic β strands, an elastic shortening of a non-β-sheet region, or a ratcheting down of overlapping regions of the amphipathic β-sheet belts. In any case, as the particle size decreases, progressively greater numbers of amphipathic helices associate with the LDL surface lipid to maintain surface pressures within an acceptable range.

On the other hand, no more than 40% of the lipid-associating amphipathic α-helices of apoB-100 appear suited to reverse their lipid association between different LDL subclasses; the majority have a high enough lipid affinity to be considered permanently associated with the LDL particle surface (Table 2). In a recent review, Hevonoja et al. (127) proposed a model for LDL in which the amphipathic α-helices of the α_2 domain create a "spring"-like structure at the junction of the β_1 and β_2 amphipathic β-sheet domains that regulates LDL particle size. The α_2 domain contains approximately 12 amphipathic helices with presumed permanent lipid association (i.e., those with a $\Lambda\alpha \geq 12$) that could form the spring-like structure. However, the proposed model involves a picket fence arrangement of amphipathic helices. Because the picket fence model for antiparallel helix-helix interactions in discoidal HDL appears not to be correct (64, 135, 141–143), the molecular basis for a model like that of Hevonoja et al. (127) at present is unclear.

Consensus LDL model

In spite of the unresolved issues discussed above, there is enough information at this time to develop a low resolution consensus model for LDL. Figure 11 is a schematic of this consensus model. The left-hand sphere focuses on the proposed organization of lipid, including amphipathic β-sheet-induced lipid-core ridges (in red) containing a probable nidus of cholesteryl ester in the smectic phase (also in red), boundary phospholipid (in green) and, for reference to the right-hand sphere, amphipathic β sheets (in blue).

The right-hand sphere illustrates the proposed organization of apoB-100 on the LDL particle surface. The β barrel (blue): antiparallel α-helix (red) structure for the N-terminal 600 residues of apoB is shown at the upper pole of this LDL particle. The next 400 residues of apoB to residue 1,000 that are homologous to two-thirds of the lipid-binding pocket of lipovitellin (βA and βB) are shown as part of the β_1 domain (blue) that forms an amphipathic β sheet extending approximately half-way around the LDL particle. The amphipathic α-helices of the α_2 domain are shown in red as being randomly distributed predominantly on the β sheet-free upper pole of the LDL particle. The β_2 domain (blue) is shown forming an amphipathic β-sheet belt extending half-way around

the LDL particle on the side opposite and slightly below the β_1 domain. Three prd postulated to form condensed structures unassociated with surface lipid in the β_2 domain are shown schematically, with no attempt to suggest a particular structure. The two β domains are arbitrarily shown as forming a smooth belt on the LDL particle surface; it is certainly possible that these two belts are not smooth, but contain kinks. Finally, the amphipathic helices of the α_3 domain are shown in red as being randomly distributed predominantly on the β sheet-free lower pole of the LDL particle. No attempt has been made to illustrate the bow proposed by Chatterton et al. (102) to be formed by the α_3 domain when it crosses over the β_2 domain near residue 3,500. The consensus model of Fig. 11 is proposed as a working guide only for future studies of LDL structure; details of the model are not intended to be taken too literally. 🔓

REFERENCES

1. Segrest, J. P., D. W. Garber, C. G. Brouillette, S. C. Harvey, and G. M. Anantharamaiah. 1994. The amphipathic alpha helix: a multifunctional structural motif in plasma apolipoproteins. *Adv. Protein Chem.* **45:** 303–369.
2. Segrest, J. P., M. K. Jones, H. De Loof, C. G. Brouillette, Y. V. Venkatachalapathi, and G. M. Anantharamaiah. 1992. The amphipathic helix in the exchangeable apolipoproteins: a review of secondary structure and function. *J. Lipid Res.* **33:** 141–166.
3. Segrest, J. P., H. De Loof, J. G. Dohlman, C. G. Brouillette, and G. M. Anantharamaiah. 1990. Amphipathic helix motif: classes and properties [published erratum appears in *Proteins*. 1991. **9(1):** 79]. *Proteins.* **8:** 103–117.
4. Knott, T. J., R. J. Pease, L. M. Powell, S. C. Wallis, S. C. Rall, Jr., T. L. Innerarity, B. Blackhart, W. H. Taylor, Y. Marcel, R. Milne, et al. 1986. Complete protein sequence and identification of structural domains of human apolipoprotein B. *Nature.* **323:** 734–738.
5. Cladaras, C., M. Hadzopoulou-Cladaras, R. T. Nolte, D. Atkinson, and V. I. Zannis. 1986. The complete sequence and structural analysis of human apolipoprotein B-100: relationship between apoB-100 and apoB-48 forms. *EMBO J.* **5:** 3495–3507.
6. Chen, S. H., C. Y. Yang, P. F. Chen, D. Setzer, M. Tanimura, W. H. Li, A. M. Gotto, Jr., and L. Chan. 1986. The complete cDNA and amino acid sequence of human apolipoprotein B-100. *J. Biol. Chem.* **261:** 12918–12921.
7. Fisher, W. R., M. G. Hammond, and G. L. Warmke. 1972. Measurements of the molecular weight variability of plasma low density lipoproteins among normals and subjects with hyper-lipoproteinemia. Demonstration of macromolecular heterogeneity. *Biochemistry.* **11:** 519–525.
8. Fisher, W. R. 1972. The structure of the lower-density lipoproteins of human plasma: newer concepts derived from studies with the analytical ultracentrifuge. *Ann. Clin. Lab. Sci.* **2:** 198–208.
9. Mateu, L., A. Tardieu, V. Luzzati, L. Aggerbeck, and A. M. Scanu. 1972. On the structure of human serum low density lipoprotein. *J. Mol. Biol.* **70:** 105–116.
10. Tardieu, A., L. Mateu, C. Sardet, B. Weiss, V. Luzzati, L. Aggerbeck, and A. M. Scanu. 1976. Structure of human serum lipoproteins in solution. II. Small-angle X-ray scattering study of HDL3 and LDL. *J. Mol. Biol.* **105:** 459–460.

11. Luzzati, V., A. Tardieu, L. Mateu, C. Sardet, H. B. Stuhrmann, L. Aggerbeck, and A. M. Scanu. 1976. X-ray and neutron small-angle scattering studies of human serum lipoproteins. *Brookhaven Symp. Biol.* **IV:** 61–77.

12. Atkinson, D., R. J. Deckelbaum, D. M. Small, and G. G. Shipley. 1977. Structure of human plasma low-density lipoproteins: molecular organization of the central core. *Proc. Natl. Acad. Sci. USA.* **74:** 1042–1046.

13. Laggner, P., and K. W. Muller. 1978. The structure of serum lipoproteins as analysed by X-ray small-angle scattering. *Q. Rev. Biophys.* **11:** 371–425.

14. Luzzati, V., A. Tardieu, and L. P. Aggerbeck. 1979. Structure of serum low-density lipoprotein. I. A solution X-ray scattering study of a hyperlipidemic monkey low-density lipoprotein. *J. Mol. Biol.* **131:** 435–473.

15. Atkinson, D., D. M. Small, and G. G. Shipley. 1980. X-ray and neutron scattering studies of plasma lipoproteins. *Ann. NY Acad. Sci.* **348:** 284–298.

16. Shen, M. M., R. M. Krauss, F. T. Lindgren, and T. M. Forte. 1981. Heterogeneity of serum low density lipoproteins in normal human subjects. *J. Lipid Res.* **22:** 236–244.

17. Krauss, R. M., and D. J. Burke. 1982. Identification of multiple subclasses of plasma low density lipoproteins in normal humans. *J. Lipid Res.* **23:** 97–104.

18. Austin, M. A., and R. M. Krauss. 1986. Genetic control of low-density-lipoprotein subclasses. *Lancet.* **2:** 592–595.

19. Krauss, R. M. 1995. Dense low density lipoproteins and coronary artery disease. *Am. J. Cardiol.* **75:** 53B–57B.

20. Campos, H., K. S. Arnold, M. E. Balestra, T. L. Innerarity, and R. M. Krauss. 1996. Differences in receptor binding of LDL subfractions. *Arterioscler. Thromb. Vasc. Biol.* **16:** 794–801.

21. McNamara, J. R., D. M. Small, Z. Li, and E. J. Schaefer. 1996. Differences in LDL subspecies involve alterations in lipid composition and conformational changes in apolipoprotein B. *J. Lipid Res.* **37:** 1924–1935.

22. Musliner, T. A., and R. M. Krauss. 1988. Lipoprotein subspecies and risk of coronary disease. *Clin. Chem.* **34:** B78–83.

23. Austin, M. A., M. C. King, K. M. Vranizan, and R. M. Krauss. 1990. Atherogenic lipoprotein phenotype. A proposed genetic marker for coronary heart disease risk [see comments]. *Circulation.* **82:** 495–506.

24. Kane, J. P. 1983. Apoprotein B: structural and metabolic heterogeneity. *Annu. Rev. Physiol.* **45:** 637–650.

25. Kane, J. P., T. Sata, R. L. Hamilton, and R. J. Havel. 1975. Apoprotein composition of very low density lipoproteins of human serum. *J. Clin. Invest.* **56:** 1622–1634.

26. Lee, D. M., A. J. Valente, W. H. Kuo, and H. Maeda. 1981. Properties of apolipoprotein B in urea and in aqueous buffers. The use of glutathione and nitrogen in its solubilization. *Biochim. Biophys. Acta.* **666:** 133–146.

27. Scanu, A., and R. Hirz. 1968. Human serum low-density lipoprotein protein: its conformation studied by circular dichroism. *Nature.* **218:** 200–201.

28. Gotto, A. M., R. I. Levy, and D. S. Fredrickson. 1968. Observations on the conformation of human beta lipoprotein: evidence for the occurrence of beta structure. *Proc. Natl. Acad. Sci. USA.* **60:** 1436–1441.

29. Chen, G. C., M. J. Chapman, and J. P. Kane. 1983. Secondary structure and thermal behavior of trypsin-treated low-density lipoproteins from human serum, studied by circular dichroism. *Biochim. Biophys. Acta.* **754:** 51–56.

30. Singh, S., and D. M. Lee. 1986. Conformational studies of lipoprotein B and apolipoprotein B: effects of disulfide reducing agents, sulfhydryl blocking agent, denaturing agents, pH and storage. *Biochim. Biophys. Acta.* **876:** 460–468.

31. Wei, C. F., S. H. Chen, C. Y. Yang, Y. L. Marcel, R. W. Milne, W. H. Li, J. T. Sparrow, A. M. Gotto, Jr., and L. Chan. 1985. Molecular cloning and expression of partial cDNAs and deduced amino acid sequence of a carboxyl-terminal fragment of human apolipoprotein B-100. *Proc. Natl. Acad. Sci. USA.* **82:** 7265–7269.

32. De Loof, H., M. Rosseneu, C. Y. Yang, W. H. Li, A. M. Gotto, Jr., and L. Chan. 1987. Human apolipoprotein B: analysis of internal repeats and homology with other apolipoproteins. *J. Lipid Res.* **28:** 1455–1465.

33. Yang, C. Y., T. W. Kim, Q. Pao, L. Chan, R. D. Knapp, A. M. Gotto, Jr., and H. J. Pownall. 1989. Structure and conformational analysis of lipid-associating peptides of apolipoprotein B-100 produced by trypsinolysis. *J. Protein Chem.* **8:** 689–699.

34. Yang, C. Y., Z. W. Gu, S. A. Weng, T. W. Kim, S. H. Chen, H. J. Pownall, P. M. Sharp, S. W. Liu, W. H. Li, A. M. Gotto, Jr., et al. 1989. Structure of apolipoprotein B-100 of human low density lipoproteins. *Arteriosclerosis.* **9:** 96–108.

35. Segrest, J. P., M. K. Jones, V. K. Mishra, G. M. Anantharamaiah, and D. W. Garber. 1994. ApoB-100 has a pentapartite structure composed of three amphipathic alpha-helical domains alternating with two amphipathic beta-strand domains. Detection by the computer program LOCATE. *Arterioscler. Thromb.* **14:** 1674–1685.

36. Chen, G. C., D. A. Hardman, R. L. Hamilton, C. M. Mendel, J. W. Schilling, S. Zhu, K. Lau, J. S. Wong, and J. P. Kane. 1989. Distribution of lipid-binding regions in human apolipoprotein B-100. *Biochemistry.* **28:** 2477–2484.

37. Goormaghtigh, E., J. De Meutter, B. Vanloo, R. Brasseur, M. Rosseneu, and J. M. Ruysschaert. 1989. Evaluation of the secondary structure of apoB-100 in low-density lipoprotein (LDL) by infrared spectroscopy. *Biochim. Biophys. Acta.* **1006:** 147–150.

38. Yang, C. Y., S. H. Chen, S. H. Gianturco, W. A. Bradley, J. T. Sparrow, M. Tanimura, W. H. Li, D. A. Sparrow, H. DeLoof, M. Rosseneu et al. 1986. Sequence, structure, receptor-binding domains and internal repeats of human apolipoprotein B-100. *Nature.* **323:** 738–742.

39. Olofsson, S. O., G. Bjursell, K. Bostrom, P. Carlsson, J. Elovson, A. A. Protter, M. A. Reuben, and G. Bondjers. 1987. Apolipoprotein B: structure, biosynthesis and role in the lipoprotein assembly process. *Atherosclerosis.* **68:** 1–17.

40. Goormaghtigh, E., V. Cabiaux, J. De Meutter, M. Rosseneu, and J. M. Ruysschaert. 1993. Secondary structure of the particle-associating domain of apolipoprotein B-100 in low-density lipoprotein by attenuated total reflection infrared spectroscopy. *Biochemistry.* **32:** 6104–6110.

41. Lins, L., R. Brasseur, M. Rosseneu, C. Y. Yang, D. A. Sparrow, J. T. Sparrow, A. M. Gotto, Jr., and J. M. Ruysschaert. 1994. Structure and orientation of apo B-100 peptides into a lipid bilayer. *J. Protein Chem.* **13:** 77–88.

42. Nolte, R. T. 1994. Structural Analysis of the Human Apolipoproteins: An Integrated Approach Utilizing Physical and Computational Methods. PhD Dissertation. Boston University, Boston, MA.

43. Osterman, D. G., and E. T. Kaiser. 1985. Design and characterization of peptides with amphiphilic beta-strand structures. *J. Cell. Biochem.* **29:** 57–72.

44. Segrest, J. P., M. K. Jones, V. K. Mishra, V. Pierotti, S. H. Young, J. Boren, T. L. Innerarity, and N. Dashti. 1998. Apolipoprotein B-100: conservation of lipid-associating amphipathic secondary structural motifs in nine species of vertebrates. *J. Lipid Res.* **39:** 85–102.

45. Young, S. G. 1990. Recent progress in understanding apolipoprotein B. *Circulation.* **82:** 1574–1594.

46. Linton, M. F., R. V. Farese, Jr., and S. G. Young. 1993. Familial hypobetalipoproteinemia. *J. Lipid Res.* **34:** 521–541.

47. Parhofer, K. G., P. H. Barrett, C. A. Aguilar-Salinas, and G. Schonfeld. 1996. Positive linear correlation between the length of truncated apolipoprotein B and its secretion rate: in vivo studies in human apoB-89, apoB-75, apoB-54.8, and apoB-31 heterozygotes. *J. Lipid Res.* **37:** 844–852.

48. Graham, D. L., T. J. Knott, T. C. Jones, R. J. Pease, C. R. Pullinger, and J. Scott. 1991. Carboxyl-terminal truncation of apolipoprotein B results in gradual loss of the ability to form buoyant lipoproteins in cultured human and rat liver cell lines. *Biochemistry.* **30:** 5616–5621.

49. Yao, Z. M., B. D. Blackhart, M. F. Linton, S. M. Taylor, S. G. Young, and B. J. McCarthy. 1991. Expression of carboxyl-terminally truncated forms of human apolipoprotein B in rat hepatoma cells. Evidence that the length of apolipoprotein B has a major effect on the buoyant density of the secreted lipoproteins. *J. Biol Chem.* **266:** 3300–3308.

50. Spring, D. J., L. W. Chen-Liu, J. E. Chatterton, J. Elovson, and V. N. Schumaker. 1992. Lipoprotein assembly. Apolipoprotein B size determines lipoprotein core circumference. *J. Biol. Chem.* **267:** 14839–14845.

51. McLeod, R. S., Y. Zhao, S. L. Selby, J. Westerlund, and Z. Yao. 1994. Carboxyl-terminal truncation impairs lipid recruitment by apolipoprotein B100 but does not affect secretion of the truncated apolipoprotein B-containing lipoproteins. *J. Biol. Chem.* **269:** 2852–2862.

52. Carraway, M., H. Herscovitz, V. Zannis, and D. M. Small. 2000. Specificity of lipid incorporation is determined by sequences in the N-terminal 37 of apoB. *Biochemistry.* **39:** 9737–9745.

53. Gantz, D. L., M. T. Walsh, and D. M. Small. 2000. Morphology of

sodium deoxycholate-solubilized apolipoprotein B-100 using negative stain and vitreous ice electron microscopy. *J. Lipid Res.* **41:** 1464–1472.

54. Small, D. M., and D. Atkinson. 1997. The first beta sheet region of apoB (apoB21–41) is a amphipathic ribbon 50–60 Å wide and 200 Å long which initiates triglyceride binding and assembly of nascent lipoproteins. *Circulation.* **96:** 1.

55. Nolte, R. T., and D. Atkinson. 1992. Conformational analysis of apolipoprotein A-I and E-3 based on primary sequence and circular dichroism. *Biophys. J.* **63:** 1221–1239.

56. White, J. V., C. M. Stultz, and T. F. Smith. 1994. Protein classification by stochastic modeling and optimal filtering of amino-acid sequences. *Math. Biosci.* **119:** 35–75.

57. Raag, R., K. Appelt, N. H. Xuong, and L. Banaszak. 1988. Structure of the lamprey yolk lipid-protein complex lipovitellin-phosvitin at 2.8 Å resolution. *J. Mol. Biol.* **200:** 553–569.

58. Anderson, T. A., D. G. Levitt, and L. J. Banaszak. 1998. The structural basis of lipid interactions in lipovitellin, a soluble lipoprotein. *Structure.* **6:** 895–909.

59. Segrest, J. P., M. K. Jones, and N. Dashti. 1999. N-terminal domain of apolipoprotein B has structural homology to lipovitellin and microsomal triglyceride transfer protein: a "lipid pocket" model for self-assembly of apoB-containing lipoprotein particles. *J. Lipid Res.* **40:** 1401–1416.

60. Schumaker, V. N., M. L. Phillips, and J. E. Chatterton. 1994. Apolipoprotein B and low-density lipoprotein structure: implications for biosynthesis of triglyceride-rich lipoproteins. *Adv. Protein Chem.* **45:** 205–248.

61. Shelness, G. S., and J. T. Thornburg. 1996. Role of intramolecular disulfide bond formation in the assembly and secretion of apolipoprotein B-100-containing lipoproteins. *J. Lipid Res.* **37:** 408–419.

62. Huang, X. F., and G. S. Shelness. 1997. Identification of cysteine pairs within the amino-terminal 5% of apolipoprotein B essential for hepatic lipoprotein assembly and secretion. *J. Biol. Chem.* **272:** 31872–31876.

63. Ingram, M. F., and G. S. Shelness. 1997. Folding of the amino-terminal domain of apolipoprotein B initiates microsomal triglyceride transfer protein-dependent lipid transfer to nascent very low density lipoprotein. *J. Biol. Chem.* **272:** 10279–10286.

64. Segrest, J. P., L. Li, G. M. Anantharamaiah, S. C. Harvey, K. N. Liadaki, and V. Zannis. 2000. Structure and function of apolipoprotein A-I and high-density lipoprotein. *Curr. Opin. Lipidol.* **11:** 105–115.

65. Wetterau, J. R., L. P. Aggerbeck, M. E. Bouma, C. Eisenberg, A. Munck, M. Hermier, J. Schmitz, G. Gay, D. J. Rader, and R. E. Gregg. 1992. Absence of microsomal triglyceride transfer protein in individuals with abetalipoproteinemia. *Science.* **258:** 999–1001.

66. Herscovitz, H., M. Hadzopoulou-Cladaras, M. T. Walsh, C. Cladaras, V. I. Zannis, and D. M. Small. 1991. Expression, secretion, and lipid-binding characterization of the N-terminal 17% of apolipoprotein B [published erratum appears in *Proc. Natl. Acad. Sci. USA.* 1991. **88(20):** 9375]. *Proc. Natl. Acad. Sci. USA.* **88:** 7313–7317.

67. Gordon, D. A., H. Jamil, D. Sharp, D. Mullaney, Z. Yao, R. E. Gregg, and J. Wetterau. 1994. Secretion of apolipoprotein B-containing lipoproteins from HeLa cells is dependent on expression of the microsomal triglyceride transfer protein and is regulated by lipid availability. *Proc. Natl. Acad. Sci. USA.* **91:** 7628–7632.

68. Jamil, H., D. A. Gordon, D. C. Eustice, C. M. Brooks, J. K. Dickson, Jr., Y. Chen, B. Ricci, C. H. Chu, T. W. Harrity, C. P. Ciosek, Jr., S. A. Biller, R. E. Gregg, and J. R. Wetterau. 1996. An inhibitor of the microsomal triglyceride transfer protein inhibits apoB secretion from HepG2 cells. *Proc. Natl. Acad. Sci. USA.* **93:** 11991–11995.

69. Gretch, D. G., S. L. Sturley, L. Wang, B. A. Lipton, A. Dunning, K. A. Grunwald, J. R. Wetterau, Z. Yao, P. Talmud, and A. D. Attie. 1996. The amino terminus of apolipoprotein B is necessary but not sufficient for microsomal triglyceride transfer protein responsiveness. *J. Biol. Chem.* **271:** 8682–8691.

70. Jamil, H., C. H. Chu, J. K. Dickson, Jr., Y. Chen, M. Yan, S. A. Biller, R. E. Gregg, J. R. Wetterau, and D. A. Gordon. 1998. Evidence that microsomal triglyceride transfer protein is limiting in the production of apolipoprotein B-containing lipoproteins in hepatic cells. *J. Lipid Res.* **39:** 1448–1454.

71. Liao, W., and L. Chan. 2000. Apolipoprotein B, a paradigm for proteins regulated by intracellular degradation, does not undergo intracellular degradation in CaCo2 cells. *J. Biol. Chem.* **275:** 3950–3956.

72. Banaszak, L., W. Sharrock, and P. Timmins. 1991. Structure and function of a lipoprotein: lipovitellin. *Annu. Rev. Biophys. Biophys. Chem.* **20:** 221–246.

73. Sharrock, W. J., T. A. Rosenwasser, J. Gould, J. Knott, D. Hussey, J. I. Gordon, and L. Banaszak. 1992. Sequence of lamprey vitellogenin. Implications for the lipovitellin crystal structure. *J. Mol. Biol.* **226:** 903–907.

74. Bradbury, P., C. J. Mann, S. Kochl, T. A. Anderson, S. A. Chester, J. M. Hancock, P. J. Ritchie, J. Amey, G. B. Harrison, D. G. Levitt, L. J. Banaszak, J. Scott, and C. C. Shoulders. 1999. A common binding site on the microsomal triglyceride transfer protein for apolipoprotein B and protein disulfide isomerase. *J. Biol. Chem.* **274:** 3159–3164.

75. Mann, C. J., T. A. Anderson, J. Read, S. A. Chester, G. B. Harrison, S. Kochl, P. J. Ritchie, P. Bradbury, F. S. Hussain, J. Amey, B. Vanloo, M. Rosseneu, R. Infante, J. M. Hancock, D. G. Levitt, L. J. Banaszak, J. Scott, and C. C. Shoulders. 1999. The structure of vitellogenin provides a molecular model for the assembly and secretion of atherogenic lipoproteins. *J. Mol. Biol.* **285:** 391–408.

76. Babin, P. J., J. Bogerd, F. P. Kooiman, W. J. Van Marrewijk, and D. J. Van der Horst. 1999. Apolipophorin II/I, apolipoprotein B, vitellogenin, and microsomal triglyceride transfer protein genes are derived from a common ancestor. *J. Mol. Evol.* **49:** 150–160.

77. Hussain, M. M., A. Bakillah, N. Nayak, and G. S. Shelness. 1998. Amino acids 430–570 in apolipoprotein B are critical for its binding to microsomal triglyceride transfer protein. *J. Biol. Chem.* **273:** 25612–25615.

78. Nicodeme, E., F. Benoist, R. McLeod, Z. Yao, J. Scott, C. C. Shoulders, and T. Grand-Perret. 1999. Identification of domains in apolipoprotein B100 that confer a high requirement for the microsomal triglyceride transfer protein. *J. Biol. Chem.* **274:** 1986–1993.

79. Boren, J., A. White, M. Wettesten, J. Scott, L. Graham, and S. O. Olofsson. 1991. The molecular mechanism for the assembly and secretion of apoB-100-containing lipoproteins. *Prog. Lipid Res.* **30:** 205–218.

80. McLeod, R. S., Y. Wang, S. Wang, A. Rusinol, P. Links, and Z. Yao. 1996. Apolipoprotein B sequence requirements for hepatic very low density lipoprotein assembly. Evidence that hydrophobic sequences within apolipoprotein B-48 mediate lipid recruitment. *J. Biol. Chem.* **271:** 18445–18455.

81. Hospattankar, A. V., S. W. Law, K. Lackner, and H. B. Brewer, Jr. 1986. Identification of low density lipoprotein receptor binding domains of human apolipoprotein B-100: a proposed consensus LDL receptor binding sequence of apoB-100. *Biochem. Biophys. Res. Commun.* **139:** 1078–1085.

82. De Loof, H., M. Rosseneu, R. Brasseur, and J. M. Ruysschaert. 1986. Use of hydrophobicity profiles to predict receptor binding domains on apolipoprotein E and the low density lipoprotein apolipoprotein B-E receptor. *Proc. Natl. Acad. Sci. USA.* **83:** 2295–2299.

83. Weisgraber, K. H. 1994. Apolipoprotein E: structure-function relationships. *Adv. Protein Chem.* **45:** 249–302.

84. Milne, R., R. Theolis, Jr., R. Maurice, R. J. Pease, P. K. Weech, E. Rassart, J. C. Fruchart, J. Scott, and Y. L. Marcel. 1989. The use of monoclonal antibodies to localize the low density lipoprotein receptor-binding domain of apolipoprotein B. *J. Biol. Chem.* **264:** 19754–19760.

85. Law, A., and J. Scott. 1990. A cross-species comparison of the apolipoprotein B domain that binds to the LDL receptor. *J. Lipid Res.* **31:** 1109–1120.

86. Welty, F. K., L. Seman, and F. T. Yen. 1995. Purification of the apolipoprotein B-67-containing low density lipoprotein particle and its affinity for the low density lipoprotein receptor. *J. Lipid Res.* **36:** 2622–2629.

87. Krul, E. S., K. G. Parhofer, P. H. Barrett, R. D. Wagner, and G. Schonfeld. 1992. ApoB-75, a truncation of apolipoprotein B associated with familial hypobetalipoproteinemia: genetic and kinetic studies. *J. Lipid Res.* **33:** 1037–1050.

88. Boren, J., I. Lee, W. Zhu, K. Arnold, S. Taylor, and T. L. Innerarity. 1998. Identification of the low density lipoprotein receptor-binding site in apolipoprotein B100 and the modulation of its binding activity by the carboxyl terminus in familial defective apo-B100. *J. Clin. Invest.* **101:** 1084–1093.

89. Innerarity, T. L., R. W. Mahley, K. H. Weisgraber, T. P. Bersot, R. M. Krauss, G. L. Vega, S. M. Grundy, W. Friedl, J. Davignon, and B. J. McCarthy. 1990. Familial defective apolipoprotein B-100: a mutation of apolipoprotein B that causes hypercholesterolemia. *J. Lipid Res.* **31:** 1337–1349.

90. Chen, Z., J. E. Saffitz, M. A. Latour, and G. Schonfeld. 1999. Truncated apo B-70.5-containing lipoproteins bind to megalin but not the LDL receptor. *J. Clin Invest.* **103:** 1419–1430.

91. Willnow, T. E. 1999. The low-density lipoprotein receptor gene family: multiple roles in lipid metabolism [see comments]. *J. Mol. Med.* **77:** 306–315.

92. Williams, K. J., and I. Tabas. 1995. The response-to-retention hypothesis of early atherogenesis. *Arterioscler. Thromb. Vasc. Biol.* **15:** 551–561.

93. Weisgraber, K. H., and S. C. Rall, Jr. 1987. Human apolipoprotein B-100 heparin-binding sites. *J. Biol. Chem.* **262:** 11097–11103.

94. Hirose, N., D. T. Blankenship, M. A. Krivanek, R. L. Jackson, and A. D. Cardin. 1987. Isolation and characterization of four heparin-binding cyanogen bromide peptides of human plasma apolipoprotein B. *Biochemistry.* **26:** 5505–5512.

95. Shih, I. L., R. S. Lees, M. Y. Chang, and A. M. Lees. 1990. Focal accumulation of an apolipoprotein B-based synthetic oligopeptide in the healing rabbit arterial wall. *Proc. Natl. Acad. Sci. USA.* **87:** 1436–1440.

96. Olsson, U., G. Camejo, E. Hurt-Camejo, K. Elfsber, O. Wiklund, and G. Bondjers. 1997. Possible functional interactions of apolipoprotein B-100 segments that associate with cell proteoglycans and the ApoB/E receptor. *Arterioscler. Thromb. Vasc. Biol.* **17:** 149–155.

97. Goldberg, I. J., W. D. Wagner, L. Pang, L. Paka, L. K. Curtiss, J. A. DeLozier, G. S. Shelness, C. S. H. Young, and S. Pillarisetti. 1998. The NH2-terminal region of apolipoprotein B is sufficient for lipoprotein association with glycosaminoglycans. *J. Biol. Chem.* **273:** 35355–35361.

98. Boren, J., K. Olin, I. Lee, A. Chait, T. N. Wight, and T. L. Innerarity. 1998. Identification of the principal proteoglycan-binding site in LDL. A single-point mutation in apo-B100 severely affects proteoglycan interaction without affecting LDL receptor binding. *J. Clin. Invest.* **101:** 2658–2664.

99. Forgez, P., H. Gregory, J. A. Young, T. Knott, J. Scott, and M. J. Chapman. 1986. Identification of surface-exposed segments of apolipoprotein B-100 in the LDL particle. *Biochem. Biophys. Res. Commun.* **140:** 250–257.

100. Babin, P. J., F. Deryckere, and F. Gannon. 1995. Presence of an extended duplication in the putative low-density-lipoprotein receptor-binding domain of apolipoprotein B. Cloning and characterization of the domain in salmon. *Eur. J. Biochem.* **230:** 45–51.

101. Fainaru, M., Z. Schafer, D. Gavish, A. Harel, and M. Schwartz. 1988. Interactions between human and carp (*Cyprimus carpio*) low density lipoproteins (LDL) and LDL receptors. *Comp. Biochem. Physiol [B].* **91:** 331–338.

102. Chatterton, J. E., M. L. Phillips, L. K. Curtiss, R. Milne, J. C. Fruchart, and V. N. Schumaker. 1995. Immunoelectron microscopy of low density lipoproteins yields a ribbon and bow model for the conformation of apolipoprotein B on the lipoprotein surface. *J. Lipid Res.* **36:** 2027–2037.

103. Gulik-Krzywicki, T., M. Yates, and L. P. Aggerbeck. 1979. Structure of serum low-density lipoprotein. II. A freeze-etching electron microscopy study. *J. Mol. Biol.* **131:** 475–484.

104. Deckelbaum, R. J., G. G. Shipley, D. M. Small, R. S. Lees, and P. K. George. 1975. Thermal transitions in human plasma low density lipoproteins. *Science.* **190:** 392–394.

105. Sears, B., R. J. Deckelbaum, M. J. Janiak, G. G. Shipley, and D. M. Small. 1976. Temperature-dependent 13C nuclear magnetic resonance studies of human serum low density lipoproteins. *Biochemistry.* **15:** 4151–4157.

106. Deckelbaum, R. J., G. G. Shipley, and D. M. Small. 1977. Structure and interactions of lipids in human plasma low density lipoproteins. *J. Biol. Chem.* **252:** 744–754.

107. Sklar, L. A., I. F. Craig, and H. J. Pownall. 1981. Induced circular dichroism of incorporated fluorescent cholesteryl esters and polar lipids as a probe of human serum low density lipoprotein structure and melting. *J. Biol. Chem.* **256:** 4286–4292.

108. Kroon, P. A. 1981. The order-disorder transition of the core cholesteryl esters of human plasma low density lipoprotein. A proton nuclear magnetic resonance study. *J. Biol. Chem.* **256:** 5332–5339.

109. Kroon, P. A., and J. Seidenberg. 1982. Organization of the core lipids of lipoproteins from normal and cholesterol-fed rabbits. A proton nuclear magnetic resonance study. *Biochemistry.* **21:** 6483–6488.

110. Parks, J. S., and H. Hauser. 1996. Low density lipoprotein particle size and core cholesteryl ester physical state affect the proton NMR magnetic environment of fatty acid methylene and methyl nuclei. *J. Lipid Res.* **37:** 1289–1297.

111. Pregetter, M., R. Prassl, B. Schuster, M. Kriechbaum, F. Nigon, J. Chapman, and P. Laggner. 1999. Microphase separation in low density lipoproteins. Evidence for a fluid triglyceride core below the lipid melting transition. *J. Biol. Chem.* **274:** 1334–1341.

112. Van Antwerpen, R., and J. C. Gilkey. 1994. Cryo-electron microscopy reveals human low density lipoprotein substructure. *J. Lipid Res.* **35:** 2223–2231.

113. van Antwerpen, R., G. C. Chen, C. R. Pullinger, J. P. Kane, M. LaBelle, R. M. Krauss, C. Luna-Chavez, T. M. Forte, and J. C. Gilkey. 1997. Cryo-electron microscopy of low density lipoprotein and reconstituted discoidal high density lipoprotein: imaging of the apolipoprotein moiety. *J. Lipid Res.* **38:** 659–669.

114. van Antwerpen, R., M. La Belle, E. Navratilova, and R. M. Krauss. 1999. Structural heterogeneity of apoB-containing serum lipoproteins visualized using cryo-electron microscopy. *J. Lipid Res.* **40:** 1827–1836.

115. Spin, J. M., and D. Atkinson. 1995. Cryoelectron microscopy of low density lipoprotein in vitreous ice. *Biophys. J.* **68:** 2115–2123.

116. Orlova, E. V., M. B. Sherman, W. Chiu, H. Mowri, L. C. Smith, and A. M. Gotto, Jr. 1999. Three-dimensional structure of low density lipoproteins by electron cryomicroscopy. *Proc. Natl. Acad. Sci. USA.* **96:** 8420–8425.

117. Prassl, R., J. M. Chapman, F. Nigon, M. Sara, S. Eschenburg, C. Betzel, A. Saxena, and P. Laggner. 1996. Crystallization and preliminary X-ray analysis of a low density lipoprotein from human plasma. *J. Biol. Chem.* **271:** 28731–28733.

118. Ritter, S., I. Frey, K. Diederichs, D. Grathwohl, J. Keul, and M. W. Baumstark. 1997. Crystallization and preliminary X-ray diffraction data of two different human low-density lipoprotein (LDL) subfractions. *Proteins.* **28:** 293–297.

119. Lunin, V. Y., N. L. Lunina, S. Ritter, I. Frey, A. Berg, K. Diederichs, A. D. Podjarny, A. Urzhumtsev, and M. W. Baumstark. 2001. Low-resolution data analysis for low-density lipoprotein particle. *Acta. Crystallogr. D. Biol. Crystallogr.* **57:** 108–121.

120. Palgunachari, M. N., V. K. Mishra, S. Lund-Katz, M. C. Phillips, S. O. Adeyeye, S. Alluri, G. M. Anantharamaiah, and J. P. Segrest. 1996. Only the two end helixes of eight tandem amphipathic helical domains of human apo A-I have significant lipid affinity. Implications for HDL assembly. *Arterioscler. Thromb. Vasc. Biol.* **16:** 328–338.

121. Mishra, V. K., and M. N. Palgunachari. 1996. Interaction of model class A1, class A2, and class Y amphipathic helical peptides with membranes. *Biochemistry.* **35:** 11210–11220.

122. Hristova, K., W. C. Wimley, V. K. Mishra, G. M. Anantharamaiah, J. P. Segrest, and S. H. White. 1999. An amphipathic alpha-helix at a membrane interface: a structural study using a novel X-ray diffraction method. *J. Mol. Biol.* **290:** 99–117.

123. Brouillette, C. G., J. P. Segrest, T. C. Ng, and J. L. Jones. 1982. Minimal size phosphatidylcholine vesicles: effects of radius of curvature on head group packing and conformation. *Biochemistry.* **21:** 4569–4575.

124. Wetterau, J. R., and A. Jonas. 1982. Effect of dipalmitoylphosphatidylcholine vesicle curvature on the reaction with human apolipoprotein A-I. *J. Biol. Chem.* **257:** 10961–10966.

125. Segrest, J. P. 1976. Molecular packing of high density lipoproteins: a postulated functional role. *FEBS Lett.* **69:** 111–115.

126. Saito, H., T. Minamida, I. Arimoto, T. Handa, and K. Miyajima. 1996. Physical states of surface and core lipids in lipid emulsions and apolipoprotein binding to the emulsion surface. *J. Biol. Chem.* **271:** 15515–15520.

127. Hevonoja, T., M. O. Pentikainen, M. T. Hyvonen, P. T. Kovanen, and M. Ala-Korpela. 2000. Structure of low density lipoprotein (LDL) particles: basis for understanding molecular changes in modified LDL. *Biochim. Biophys. Acta.* **1488:** 189–210.

128. Yeagle, P. L., R. B. Martin, L. Pottenger, and R. G. Langdon. 1978. Location and interactions of phospholipid and cholesterol in human low density lipoprotein from 31P nuclear magnetic resonance. *Biochemistry.* **17:** 2707–2710.

129. Lund-Katz, S., and M. C. Phillips. 1986. Packing of cholesterol molecules in human low-density lipoprotein. *Biochemistry.* **25:** 1562–1568.

130. Yeagle, P. L., R. G. Langdon, and R. B. Martin. 1977. Phospholipid-protein interactions in human low density lipoprotein detected by 31P nuclear magnetic resonance. *Biochemistry.* **16:** 3487–3491.

131. Cushley, R. J., W. D. Treleaven, Y. I. Parmar, R. S. Chana, and D. B. Fenske. 1987. Surface diffusion in human serum lipoproteins. *Biochem. Biophys. Res. Commun.* **146:** 1139–1145.

132. Murphy, H. C., M. Ala-Korpela, J. J. White, A. Raoof, J. D. Bell, M. L. Barnard, S. P. Burns, and R. A. Iles. 1997. Evidence for distinct behaviour of phosphatidylcholine and sphingomyelin at the

low density lipoprotein surface. *Biochem. Biophys. Res. Commun.* **234:** 733–737.

133. Murphy, H. C., S. P. Burns, J. J. White, J. D. Bell, and R. A. Iles. 2000. Investigation of human low-density lipoprotein by (1)H nuclear magnetic resonance spectroscopy: mobility of phosphatidylcholine and sphingomyelin headgroups characterizes the surface layer. *Biochemistry.* **39:** 9763–9770.

134. Ibdah, J. A., S. Lund-Katz, and M. C. Phillips. 1989. Molecular packing of high-density and low-density lipoprotein surface lipids and apolipoprotein A-I binding. *Biochemistry.* **28:** 1126–1133.

135. Segrest, J. P., M. K. Jones, A. E. Klon, C. J. Sheldahl, M. Hellinger, H. De Loof, and S. C. Harvey. 1999. A detailed molecular belt model for apolipoprotein A-I in discoidal high density lipoprotein. *J. Biol. Chem.* **274:** 31755–31758.

136. Deckelbaum, R. J., A. R. Tall, and D. M. Small. 1977. Interaction of cholesterol ester and triglyceride in human plasma very low density lipoprotein. *J. Lipid Res.* **18:** 164–168.

137. Baumstark, M. W., W. Kreutz, A. Berg, I. Frey, and J. Keul. 1990. Structure of human low-density lipoprotein subfractions, determined by X-ray small-angle scattering. *Biochim. Biophys. Acta.* **1037:** 48–57.

138. Steyrer, E., D. L. Barber, and W. J. Schneider. 1990. Evolution of lipoprotein receptors. The chicken oocyte receptor for very low density lipoprotein and vitellogenin binds the mammalian ligand apolipoprotein E. *J. Biol. Chem.* **265:** 19575–19581.

139. Perez, L. E., M. J. Fenton, and I. P. Callard. 1991. Vitellogenin—homologs of mammalian apolipoproteins? *Comp. Biochem. Physiol. [B].* **100:** 821–826.

140. Jacobs, R. E., and S. H. White. 1989. The nature of the hydrophobic binding of small peptides at the bilayer interface: implications for the insertion of transbilayer helices. *Biochemistry.* **28:** 3421–3437.

141. Koppaka, V., and P. H. Axelsen. 1999. Lipoprotein A-I structure. *Trends Cardiovasc. Med.* **9:** 192–195.

142. Koppaka, V., L. Silvestro, J. A. Engler, C. G. Brouillette, and P. H. Axelsen. 1999. The structure of human lipoprotein A-I. Evidence for the "belt" model. *J. Biol. Chem.* **274:** 14541–14544.

143. Klon, A. E., M. K. Jones, J. P. Segrest, and S. C. Harvey. 2000. Molecular belt models for the apolipoprotein A-I paris and milano mutations [in process citation]. *Biophys. J.* **79:** 1679–1685.

144. Ibdah, J. A., and M. C. Phillips. 1988. Effects of lipid composition and packing on the adsorption of apolipoprotein A-I to lipid monolayers. *Biochemistry.* **27:** 7155–7162.

145. Sayle, R. A., and E. J. Milner-White. 1995. RASMOL: biomolecular graphics for all. *Trends Biochem. Sci.* **20:** 374.

146. Schuler, G. D., S. F. Altschul, and D. J. Lipman. 1991. A workbench for multiple alignment construction and analysis. *Proteins.* **9:** 180–190.

147. Lawrence, C. E., S. F. Altschul, M. S. Boguski, J. S. Liu, A. F. Neuwald, and J. C. Wootton. 1993. Detecting subtle sequence signals: a Gibbs sampling strategy for multiple alignment. *Science.* **262:** 208–214.